Comparison of average stress drop measures for ruptures with heterogeneous stress change and implications for earthquake physics

Hiroyuki Noda,[1,*] Nadia Lapusta[1,2] and Hiroo Kanamori[1]

[1]*Division of Geological and Planetary Sciences, California Institute of Technology, 1200 E California Blvd., Pasadena, CA 91125, USA.*
E-mail: hnoda@jamstec.go.jp
[2]*Division of Engineering and Applied Science, California Institute of Technology, 1200 E California Blvd., Pasadena, CA 91125, USA*

SUMMARY

Stress drop, a measure of static stress change in earthquakes, is the subject of numerous investigations. Stress drop in an earthquake is likely to be spatially varying over the fault, creating a stress drop distribution. Representing this spatial distribution by a single number, as commonly done, implies averaging in space. In this study, we investigate similarities and differences between three different averages of the stress drop distribution used in earthquake studies. The first one, $\overline{\Delta\sigma}_M$, is the commonly estimated stress drop based on the seismic moment and fault geometry/dimensions. It is known that $\overline{\Delta\sigma}_M$ corresponds to averaging the stress drop distribution with the slip distribution due to uniform stress drop as the weighting function. The second one, $\overline{\Delta\sigma}_A$, is the simplest (unweighted) average of the stress drop distribution over the fault, equal to the difference between the average stress levels on the fault before and after an earthquake. The third one, $\overline{\Delta\sigma}_E$, enters discussions of energy partitioning and radiation efficiency; we show that it corresponds to averaging the stress drop distribution with the actual final slip at each point as the weighting function. The three averages, $\overline{\Delta\sigma}_M$, $\overline{\Delta\sigma}_A$, and $\overline{\Delta\sigma}_E$, are often used interchangeably in earthquake studies and simply called 'stress drop'. Yet they are equal to each other only for ruptures with spatially uniform stress drop, which results in an elliptical slip distribution for a circular rupture. Indeed, we find that other relatively simple slip shapes—such as triangular, trapezoidal or sinusoidal—already result in stress drop distributions with notable differences between $\overline{\Delta\sigma}_M$, $\overline{\Delta\sigma}_A$, and $\overline{\Delta\sigma}_E$. Introduction of spatial slip heterogeneity results in further systematic differences between them, with $\overline{\Delta\sigma}_E$ always being larger than $\overline{\Delta\sigma}_M$, a fact that we have proven theoretically, and $\overline{\Delta\sigma}_A$ almost always being the smallest. In particular, the value of the energy-related $\overline{\Delta\sigma}_E$ significantly increases in comparison to the moment-based $\overline{\Delta\sigma}_M$ with increasing roughness of the slip distribution over the fault. Previous studies used $\overline{\Delta\sigma}_M$ in place of $\overline{\Delta\sigma}_E$ in computing the radiation ratio η_R that compares the radiated energy in earthquakes to a characteristic part of their strain energy change. Typical values of η_R for large earthquakes were found to be from 0.25 to 1. Our finding that $\overline{\Delta\sigma}_E \geq \overline{\Delta\sigma}_M$ allows us to interpret the values of η_R as the upper bound. We determine the restrictions placed by such estimates on the evolution of stress with slip at the earthquake source. We also find that $\overline{\Delta\sigma}_E$ can be approximated by $\overline{\Delta\sigma}_M$ if the latter is computed based on a reduced rupture area.

Key words: Earthquake dynamics; Dynamics and mechanics of faulting; Fractures and faults.

1 INTRODUCTION

Since earthquakes lead to the overall reduction of stress on the ruptured fault domain, stress drop is an important physical pa-

∗ Now at: Institute for Research on Earth Evolution, Japan Agency for Marine-Earth Science and Technology, 3173-25 Showa-machi, Kanazawa-ku, Yokohama, Kanagawa, 236-0001 Japan
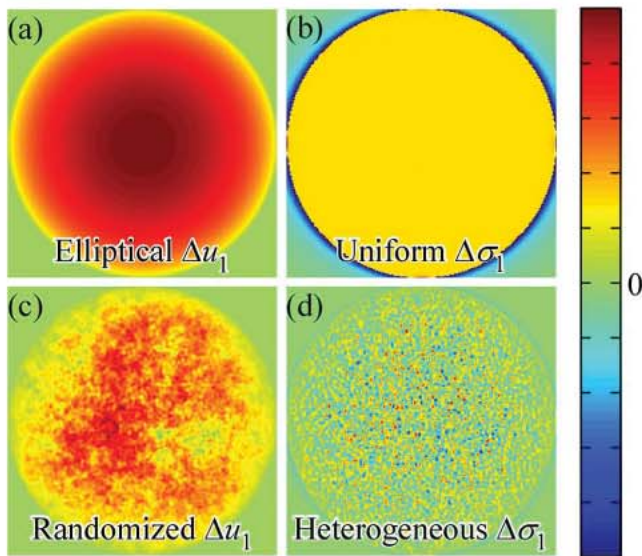
rameter which has long been studied in seismology (e.g. Knopoff 1958; Kanamori & Anderson 1975; Abercrombie 1995; Allmann & Shearer 2009). Most investigations report a single value for the stress drop in an earthquake. Such a single value of stress drop for the entire rupture can be interpreted unambiguously only when the stress drop is constant (i.e. spatially uniform) over the ruptured domain (Figs 1a and b). In real earthquakes, the stress drop most likely varies locally over the ruptured fault domain (e.g. Bouchon 1997), creating a spatially varying stress drop distribution. A synthetic

Figure 1. Illustration of slip distributions and the corresponding stress drop distributions for the cases of uniform and non-uniform stress drops. Yellow and red colours indicate positive values, whereas blue colours indicate negative values. (a) Slip distribution of a circular crack model with uniform stress drop. (b) The resulting stress drop distribution is uniform within the slipped circular region, with the negative stress drop (or stress increase) outside the slipped region. (c) An example of a randomized slip distribution (see Section 3.1 for details). (d) The corresponding heterogeneous stress drop distribution.

example of variable stress drop over the fault is shown in Fig. 1(d). This stress drop distribution is obtained by first constructing a randomized slip distribution motivated by observations of earthquake slip (Manighetti *et al.* 2005; Lavallée *et al.* 2006) by the method described in Section 3.1 (Fig. 1c), and then computing the resulting stress drop distribution using linear elasticity (Fig. 1d). Representing such a heterogeneous stress drop distribution by a single value inevitably implies some averaging in space.

Three notions of the average static stress drop are interchangeably used in earthquake studies, yet would be different for heterogeneous stress drop distributions. The first one, which we denote by $\overline{\Delta\sigma}_M$, is the commonly estimated static stress drop based on the seismic moment and fault geometry/dimensions (Section 2.1). The second one, $\overline{\Delta\sigma}_A$, is the difference between the average stress levels on the fault before and after an earthquake (Section 2.2). It enters, for example, estimates of the time needed for the area to be stressed to the average stress level that existed before the earthquake. The third one, $\overline{\Delta\sigma}_E$, is used in studies of energy partitioning and radiation efficiency (e.g. Venkataraman & Kanamori 2004; Kanamori & Rivera 2006) as discussed in Section 2.3. The three quantities, $\overline{\Delta\sigma}_M$, $\overline{\Delta\sigma}_A$ and $\overline{\Delta\sigma}_E$, are almost always used interchangeably and simply called 'stress drop'. Yet they are equal to each other only for ruptures with spatially uniform stress drop within the ruptured domain, which results in an elliptical slip distribution for a circular rupture, as shown in Figs 1(a) and (b). Note that even the uniform stress drop case is not completely uniform overall, since the slip varies within the ruptured domain—with elliptical shape for the circular domain, other shapes for other geometries—and the stress is actually increased outside the ruptured domain.

For spatially heterogeneous stress drop distributions, of the kind shown in Figs 1(c) and (d), $\overline{\Delta\sigma}_M$, $\overline{\Delta\sigma}_A$ and $\overline{\Delta\sigma}_E$ would not be the same in general since they correspond to different averaging

of the stress drop distribution. $\overline{\Delta\sigma}_M$ corresponds to averaging the stress drop distribution with the slip distribution due to uniform stress drop as the weighting function (Madariaga 1979, Section 2.1, appendix A). $\overline{\Delta\sigma}_A$ represents the simplest (unweighted) average of the stress change over the ruptured domain (Section 2.2). Finally, $\overline{\Delta\sigma}_E$ corresponds to averaging the stress drop distribution with the actual final slip at each point as the weighting function, as implied by the developments in Noda & Lapusta (2012) and shown in Section 2.3. To the best of our knowledge, this is the first study that explicitly introduces this energy-based average measure although its notion has been indirectly implied by Kostrov & Das (1988).

Hence it is important to understand how the seismologically estimated stress drops $\overline{\Delta\sigma}_M$ are related to the area-averaged stress drops $\overline{\Delta\sigma}_A$ and energy-related stress drops $\overline{\Delta\sigma}_E$. In this study, we investigate this issue by creating synthetic heterogeneous slip scenarios motivated by natural earthquakes (Manighetti *et al.* 2005; Lavallée *et al.* 2006) and comparing the three average stress drop measures $\overline{\Delta\sigma}_M$, $\overline{\Delta\sigma}_A$ and $\overline{\Delta\sigma}_E$ for these scenarios (Section 3). We find significant and systematic differences between these three average stress drop measures. The significance of our results for earthquake source physics is discussed in Section 4. We summarize our main findings in Section 5.

Note that the extent and nature of slip and stress heterogeneity on faults is a subject of active study and debate. In this work, heterogeneous slip distributions are generated by randomizing an assumed characteristic slip distribution in a manner motivated by the 2-D stochastic model by Lavallée *et al.* (2006). As discussed by Lavallée *et al.* (2006) and detailed in Section 3.1, the representation of slip heterogeneity in the model is based on the assumption that the seismic process is length scale-independent for a wide but truncated range (also see Andrews 1980). Due to physical processes acting during dynamic rupture, the slip heterogeneity may have different properties than assumed here, and, in particular, be scale-dependent (e.g. Cocco & Tinti 2008). Note that we also explore the effect of the characteristic shape of slip distribution which may result from the physics of the dynamic rupture process, making the slip distributions we consider not fully stochastic. The heterogeneous slip distributions we use serve as representative examples of how heterogeneity can affect the stress drop averages used in different applications. The developed procedures can be applied for determining effects of other representations of heterogeneity on average stress drop measures.

2 AVERAGE STRESS DROP MEASURES FOR HETEROGENEOUS STRESS CHANGE DISTRIBUTIONS

First, let us define the mathematical quantities needed to describe slip in an earthquake, the resulting stress drop distribution and its averaging. Let us consider stress changes due to rupture of a planar fault S embedded in a linear elastic infinite homogeneous medium (Fig. 2). We define a 3-D coordinate vector x with the unit basis vectors denoted by e_1, e_2 and e_3. Without loss of generality, let the fault S coincide with the $x_1 - x_3$ plane so that e_2 is normal to S. The initial distribution of the traction on S is denoted by $\tau^{ini}(x_1, x_3)$. An earthquake produces slip distribution $\Delta u(x_1, x_3)$, and the traction on S changes to $\tau^{fin}(x_1, x_3)$. Without loss of generality, let us choose e_1 to coincide with the overall slip direction (the direction parallel to the integral of $\Delta u(x_1, x_3)$ over S). Note that we are not considering fault opening; hence $\Delta u_2(x_1, x_3) = 0$ and Δu is perpendicular to e_2.
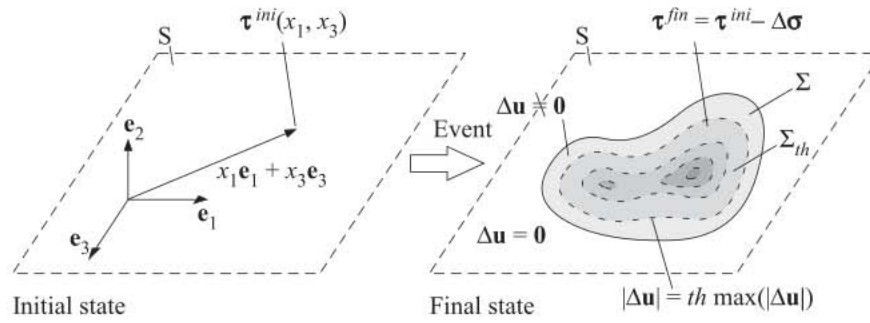
Figure 2. A schematic diagram illustrating definitions of variables in this study.

The (vector) distribution of stress drop on S, $\Delta\sigma(x_1, x_3)$, is defined as

$$\Delta\sigma(x_1, x_3) = \tau^{ini}(x_1, x_3) - \tau^{fin}(x_1, x_3). \tag{1}$$

Note that $\Delta\sigma_2(x_1, x_3) = 0$. Representing this stress drop distribution as a single scalar quantity implies averaging $\Delta\sigma$ in a particular way. Often, the averaging is desired over the ruptured domain Σ, which is defined as the domain with non-zero slip,

$$\Sigma = \{x \in S \mid \Delta u(x) \neq 0\}. \tag{2}$$

In practice, it is difficult to determine Σ accurately from seismological observations because of band-limitedness and smoothing in selecting a solution (e.g. Harris & Segall 1987; Hatzell *et al.* 1996). Furthermore, in numerical forward simulations of dynamic rupture, some frictional constitutive laws (e.g. a rate- and state-dependent friction law by Dieterich 1979) predict mathematically non-zero slip everywhere on S. Hence, let us define a truncated ruptured domain, in which we include only those regions where slip exceeds a given fraction th of the maximum slip,

$$\Sigma_{th} = \{x \mid \Delta u(x) > th \max(\Delta u)\}. \tag{3}$$

Note that $\Sigma_{th} = \Sigma$ at $th = 0$.

Both the slip distribution $\Delta u(x_1, x_3)$ and the stress drop distribution $\Delta\sigma(x_1, x_3)$ are vectors with two non-zero components, in the fault-defining directions e_1 and e_3. In many situations, slip in a single direction dominates, and in this study, this would be the overall slip direction e_1. Hence, while the various averaged quantities are defined below in terms of the vector distributions Δu and $\Delta\sigma$, components Δu_1 and $\Delta\sigma_1$ often dominate, and the terms with the other component can often be ignored.

2.1 Averaging of stress drop distribution based on seismic moment

Seismological estimates of average stress drop are based on the seismic moment M_0 and fault geometry/dimensions. In the case of faults with characteristic dimension $\rho = A^{1/2}$, the following expression is used (e.g. Kanamori & Anderson 1975; Parsons *et al.* 1988):

$$\overline{\Delta\sigma}_M = C\frac{M_0}{\rho^3} = C\frac{M_0}{A^{3/2}}, \tag{4}$$

where A is the ruptured area and C depends on the shape of the ruptured domain, for example, $C = 2.44$ for a circular ruptured domain (or crack) and $C = 2.53, 3.02$ and 5.21 for rectangular cracks with aspect ratios $\alpha = 1, 4$ and 16, respectively. For the determination of C in the rectangular cases, see Appendix B1. M_0 can be well estimated from long-period waves, and the characteristic

dimension $\rho = A^{1/2}$ can be estimated from seismic observations under certain assumptions, such as a relationship between the corner frequency and the length scale of the rupture (e.g. Aki 1967; Brune 1970; Madariaga 1976). In this study, we call such stress drop estimates moment-based or seismologically estimated.

If the actual stress drop is uniform over the ruptured domain, $\overline{\Delta\sigma}_M$ is equal to that uniform value. If the actual stress drop is heterogeneous, given by the distribution $\Delta\sigma(x_1, x_3)$, then $\overline{\Delta\sigma}_M$ gives a weighted average of $\Delta\sigma(x_1, x_3)$. The average is weighted by the slip distribution E^{12} due to the uniform stress drop in the overall slip direction e_1 over the same ruptured domain,

$$\begin{aligned}\overline{\Delta\sigma}_M &= \frac{\int_S \Delta\sigma \cdot E^{12} \, dS}{\int_S e_1 \cdot E^{12} \, dS} \\ &= \frac{\int_S \Delta\sigma_1 E_1^{12} + \Delta\sigma_3 E_3^{12} \, dS}{\int_S E_1^{12} \, dS} \\ &= \frac{\int_S \Delta\sigma \cdot w \, dS}{\int_S e_1 \cdot w \, dS}; \quad w = E^{12},\end{aligned} \tag{5}$$

where w is a weighting function. This relation was established by Madariaga (1979), as reviewed in Appendix A.

Since the overall slip is in the direction of e_1, the term in eq. (5) with E_1^{12} is expected to dominate. If the effect of E_3^{12} is negligible (as is the case for circular ruptures, for example), then $\overline{\Delta\sigma}_M$ is actually the average of the non-uniform stress change distribution $\Delta\sigma_1$ weighted by the slip function E_1^{12}. For circular ruptures, E_1^{12} has an elliptical shape, peaking in the middle of the ruptured domain Σ and going to zero at the boundaries of it. Hence this moment-based averaging would emphasize stress changes in the middle of the ruptured domain.

Note that an accurate determination of the ruptured domain Σ is difficult in practice as mentioned in the previous section. For example, smoothness constraints in finite fault inversions result in areas of near-zero slip that are often poorly constrained (e.g. Somerville *et al.* 1999). Such areas would affect the extent of the rupture and hence the stress drop estimate $\overline{\Delta\sigma}_M$. To study this effect, we use the definition of the truncated ruptured domain eq. (3) to define the corresponding threshold-dependent moment-based average stress drop $\overline{\Delta\sigma}_{Mth}$ given by

$$\overline{\Delta\sigma}_{Mth} = C\frac{M_0}{A_{th}^{3/2}}, \tag{6}$$

where A_{th} is the area of Σ_{th}. Σ_{th} can have a complex shape if the slip distribution is heterogeneous. To enable comparison to the seismologically estimated stress drops, we do not attempt to compute C for the actual complex shapes, rather using the value of C for the original (circular or rectangular) domain. Hence $\overline{\Delta\sigma}_{Mth}$ in eq. (6) depends both on the shape of the original ruptured domain that

determines C and on the threshold th. For further discussion, see Section 4.2. Note that Somerville *et al.* (1999) suggested a related but somewhat different criterion to reduce the rupture area based on slip; in their case, the domain was trimmed from outside so that it retained the rectangular shape.

2.2 Spatial average of stress drop distribution

The seismologically estimated stress drop is sometimes intuitively interpreted as the spatially averaged stress drop. There are several studies comparing the seismologically estimated stress drops and stress drops obtained in one-degree-of-freedom systems such as spring–slider systems and laboratory frictional experiments (e.g. Marone 1998; He *et al.* 2003). The former values are determined through a rather complex averaging procedure as already discussed, while the latter values are simple spatial averages over the simulated fault which is assumed to undergo uniform slip. Although such comparisons may be valid under certain conditions, it is important to understand what those conditions are.

The spatially averaged stress drop can be expressed as

$$\overline{\Delta\sigma}_A = \frac{\int_\Sigma \Delta\sigma_1 \, dS}{A} = \frac{\int_S \Delta\boldsymbol{\sigma} \cdot \boldsymbol{w} \, dS}{\int_S \boldsymbol{e}_1 \cdot \boldsymbol{w} \, dS}; \quad \boldsymbol{w} = \begin{cases} \boldsymbol{e}_1 & (\boldsymbol{x} \in \Sigma) \\ 0 & \text{otherwise} \end{cases}. \tag{7}$$

Hence, it is the average of stress change distribution $\Delta\sigma$ using a box-car function as the weighting function. Madariaga (1979) pointed out that the area-averaged stress drop $\overline{\Delta\sigma}_A$ is different from the seismologically estimated stress drop $\overline{\Delta\sigma}_M$.

Note that $\overline{\Delta\sigma}_A$ depends on the ruptured domain Σ, just like $\overline{\Delta\sigma}_M$. If Σ includes regions of near-zero slip, $\overline{\Delta\sigma}_A$ decreases. Indeed, if stress change is averaged over the entire infinite plane, the average is going to be zero. Using the area approximation in eq. (3), we can define

$$\overline{\Delta\sigma}_{Ath} = \frac{\int_{\Sigma_{th}} \Delta\sigma_1 \, dS}{A_{th}} = \frac{\int_S \Delta\boldsymbol{\sigma} \cdot \boldsymbol{w} \, dS}{\int_S \boldsymbol{e}_1 \cdot \boldsymbol{w} \, dS}; \quad \boldsymbol{w} = \begin{cases} \boldsymbol{e}_1 & (\boldsymbol{x} \in \Sigma_{th}) \\ 0 & \text{otherwise} \end{cases}, \tag{8}$$

where the stress drop is averaged over the sub domain Σ_{th}.

2.3 Averaging stress drop distribution based on energy considerations

One of the important uses of stress drop for earthquake physics is in studies of energy partitioning (e.g. Venkataraman & Kanamori 2004; Kanamori & Rivera 2006). Here, we consider the average $\overline{\Delta\sigma}_E$ of the stress drop distribution $\Delta\sigma(x_1, x_3)$ that would be rigorously consistent with that usage, and show that it corresponds to averaging the stress drop distribution with the actual final slip Δu at each point as the weighting function,

$$\overline{\Delta\sigma}_E = \frac{\int_\Sigma \Delta\boldsymbol{\sigma} \cdot \Delta\boldsymbol{u} \, dS}{\int_\Sigma \Delta u_1 \, dS} = \frac{\int_S \Delta\boldsymbol{\sigma} \cdot \boldsymbol{w} \, dS}{\int_S \boldsymbol{e}_1 \cdot \boldsymbol{w} \, dS}; \quad \boldsymbol{w} = \Delta\boldsymbol{u}. \tag{9}$$

Clearly, this expression is different from that for the moment-based stress drop average $\overline{\Delta\sigma}_M$. As for $\overline{\Delta\sigma}_M$ and $\overline{\Delta\sigma}_A$, the components of stress drop and slip in the overall slip direction $\boldsymbol{e}_1$ often dominate, in which case the expression simplifies to

$$\overline{\Delta\sigma}_E = \frac{\int_\Sigma \Delta\sigma_1 \Delta u_1 \, dS}{\int_\Sigma \Delta u_1 \, dS}. \tag{10}$$
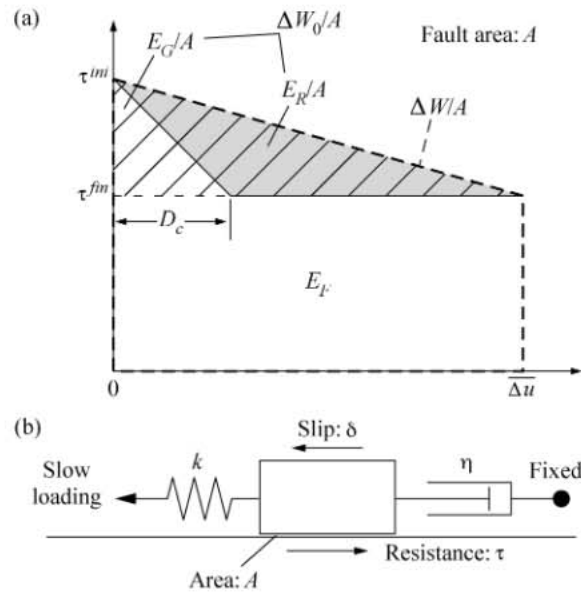

Figure 3. (a) A conceptual simplified diagram for energy partitioning in an earthquake. The marked quantities are explained in the text. (b) A one degree of freedom spring-slider-dashpot model for which the energy partitioning diagram in (a) is rigorously valid.

To understand why this is the relevant stress drop average, let us review the basics of energy partitioning studies, which are typically done in the context of a simplified conceptual diagram (Fig. 3). In the diagram, the stress on the fault drops from the initial value τ^{ini} to the final value τ^{fin} through slip D_c and then the slip proceeds at a constant stress τ^{fin} until it stops. A number of assumptions are made in this conceptual case; in particular, the initial and final stresses on the fault are assumed to be identical to the shear stress at the onset of slipping and that at the residual level, respectively. This assumption cannot be exactly true for finite-fault ruptures. First, the initial average stress before the rupture event is likely smaller than the shear stress at the onset of slipping. Secondly, the final average stress can also be different from the residual sliding resistance due to overshoot or undershoot (e.g., McGarr 1999; Kanamori & Rivera 2006). More realistic diagrams have been studied (e.g. Cocco *et al.* 2006), but let us consider this idealized case to introduce the developments of earlier studies (e.g. Venkataraman & Kanamori 2004; Kanamori & Rivera 2006).

The total strain energy release ΔW is given by

$$\Delta W = \frac{\tau^{\text{ini}} + \tau^{\text{fin}}}{2} \overline{\Delta u} A, \tag{11}$$

where $\overline{\Delta u}$ is the average slip. If $D_c = 0$, the energy dissipated on the fault plane is $E_F = \tau^{\text{fin}} \overline{\Delta u} A$ and the difference between ΔW and E_F is given by

$$\Delta W_0 = \frac{1}{2} \Delta\sigma \overline{\Delta u} A, \tag{12}$$

where $\Delta\sigma = \tau^{\text{ini}} - \tau^{\text{fin}}$.

In previous studies (e.g. Venkataraman & Kanamori 2004; Kanamori & Rivera 2006), ΔW_0 was called 'the available energy', in the sense that it is the energy available for seismic radiation and any further dissipation. In a more general energy release process (e.g. an undershoot case where the stress on the fault plane during faulting becomes smaller than the final stress τ^{fin}, as discussed in Section 4.1), the dissipation on the fault can, in fact, be smaller than the dissipation with the final shear stress E_F, and hence more energy

than ΔW_0 can be radiated. That is why we refer to ΔW_0 as a partial strain energy change.

In the context of the energy-partitioning diagram (Fig. 3), part of ΔW_0 is expended as the increased dissipation at the rupture front called fracture energy and denoted E_G, and the remainder is radiated as seismic waves. That allows us to define the radiation ratio,

$$\eta_R = E_R/\Delta W_0 = \frac{2\mu E_R}{\Delta\sigma M_0}, \tag{13}$$

where E_R is the radiated energy. η_R has been called 'radiation efficiency' (e.g. Venkataraman & Kanamori 2004), but we would like to call it 'radiation ratio' because the word 'efficiency' implies that η_R cannot exceed 1. Since ΔW_0 is only a part of strain energy release, η_R can exceed 1 in general.

The radiation ratio provides an important window into the earthquake physics (Kanamori & Rivera 2006). Its interpretation relies on the possibility of representing the average dissipative behaviour of a fault through the conceptual slip-weakening representation of Fig. 3(a), and further, on using the seismically estimated, moment-based values of stress drop for $\Delta\sigma$. However, the energy partitioning diagram of Fig. 3(a) is rigorously valid only for a one-degree-of-freedom system represented as the combination of a spring, a slider and a dashpot (Fig. 3b), with the friction under the slider described by a linear slip-weakening law. Similar one-degree-of-freedom systems (usually without a dashpot, which here is a proxy for seismic radiation, but often with other friction laws) are frequently used as analogs to earthquake faults, with stick-slip obtained in such systems being compared to earthquake sequences (e.g. Marone 1998).

The finite-fault process of dynamic rupture is much more involved. Even in the case of ruptures with spatially constant stress drop and the same slip-stress relation at each point, constructing the averaged behaviour of stress with slip is non-trivial, since different points of the fault have different slip (for example, an elliptical slip shape for a circular shear rupture). More generally, stress depends on slip through other variables, such as slip rate, state variables and temperature (e.g. Rice 2006; Dieterich 2007; Tullis 2007; Lapusta & Liu 2009; Noda & Lapusta 2010b), and hence the dependence of stress on slip will be, in general, different at different points. Noda & Lapusta (2012) proposed a rigorous way for averaging the stress-slip behaviour and constructing energy-partitioning diagrams for dynamic rupture that attempt to preserve the features of local stress-slip behaviour. This point is discussed more in Section 4.1.

To understand what kind of average of the stress drop distribution should enter eq. (12) for the radiation ratio, let us consider the rigorous computation of the partial strain energy change ΔW_0. The standard approach to compute the strain energy change is as follows. We start with two elastostatic solutions (Fig. 2): (1) the initial state, with the slip on S being 0 and traction being $\tau^{\rm ini}(x_1, x_3)$ and (2) the final state, with the slip and traction being $\Delta u(x_1, x_3)$ and $\tau^{\rm fin}(x_1, x_3)$, respectively. Since the medium is assumed to be linear elastic, all linear interpolations/extrapolations of these two solutions also satisfy linear elastostatic equations. Introducing a parameter $\lambda \in [0, 1]$, we can define a continuous set (or a virtual path) of static solutions that connects the initial state ($\lambda = 0$) and the final state ($\lambda = 1$),

$$\delta_{vp}(\lambda, x) = \lambda\Delta u,$$

$$\tau_{vp}(\lambda, x) = \lambda\tau^{\rm fin} + (1 - \lambda)\tau^{\rm ini}, \tag{14}$$

where δ_{vp} and τ_{vp} represent slip and shear traction on the fault during this virtual process, respectively. The decrease in the strain energy, which is path-independent, can be calculated by integrating

work done by the medium along this path,

$$\Delta W = \int_0^1 \frac{\mathrm{d}W}{\mathrm{d}\lambda}\,\mathrm{d}\lambda = \int_0^1 \int_\Sigma \tau_{vp} \cdot \frac{\mathrm{d}\delta_{vp}}{\mathrm{d}\lambda}\,\mathrm{d}S\mathrm{d}\lambda. \tag{15}$$

Using eq. (14), we get

$$\Delta W = \int_\Sigma \left\{\frac{1}{2}\Delta\sigma + \tau^{\rm ini}\right\} \cdot \Delta u\,\mathrm{d}S. \tag{16}$$

Partial strain energy change ΔW_0 is thus

$$\Delta W_0 = \Delta W - \int_\Sigma \tau^{\rm fin} \cdot \Delta u\,\mathrm{d}S = \frac{1}{2}\int_\Sigma \Delta\sigma \cdot \Delta u\,\mathrm{d}S. \tag{17}$$

The expression for ΔW_0 can be used to define an energy-based average measure $\overline{\Delta\sigma}_E$ of stress drop distribution $\Delta\sigma$ through

$$\Delta W_0 = \frac{1}{2}\left[\frac{\int_\Sigma \Delta\sigma \cdot \Delta u\,\mathrm{d}S}{\int_\Sigma \Delta u_1\,\mathrm{d}S}\right]\int_\Sigma \Delta u_1\,\mathrm{d}S = \frac{1}{2}\overline{\Delta\sigma}_E\overline{\Delta u_1}A, \tag{18}$$

where $\overline{\Delta\sigma}_E$ is given by

$$\overline{\Delta\sigma}_E = \frac{\int_\Sigma \Delta\sigma \cdot \Delta u\,\mathrm{d}S}{\int_\Sigma \Delta u_1\,\mathrm{d}S} = \frac{\int_S \Delta\sigma \cdot w\,\mathrm{d}S}{\int_S e_1 \cdot w\,\mathrm{d}S}; \quad w = \Delta u. \tag{19}$$

Comparing eqs (12) and (18), we see that $\overline{\Delta\sigma}_E$ is the average stress drop measure that enters the computation of ΔW_0. From eq. (19), $\overline{\Delta\sigma}_E$ represent averaging the (potentially heterogeneous) stress drop distribution over the rupture with the final slip distribution as the weighting function. Note that Δu is zero outside the ruptured domain so that extending Σ to include regions of zero slip does not affect the value of $\overline{\Delta\sigma}_E$.

For future use, let us define the following averages of the initial and final shear stress distributions,

$$\overline{\tau^{\rm ini}}_E = \frac{\int_\Sigma \tau^{\rm ini} \cdot \Delta u\,\mathrm{d}S}{\int_\Sigma \Delta u_1\,\mathrm{d}S}, \tag{20}$$

$$\overline{\tau^{\rm fin}}_E = \frac{\int_\Sigma \tau^{\rm fin} \cdot \Delta u\,\mathrm{d}S}{\int_\Sigma \Delta u_1\,\mathrm{d}S}. \tag{21}$$

These averages can be used to compute the strain energy quantities by

$$\Delta W = \frac{\left(\overline{\tau^{\rm ini}}_E + \overline{\tau^{\rm fin}}_E\right)}{2}\overline{\Delta u_1}A, \quad \Delta W_0 = \frac{\left(\overline{\tau^{\rm ini}}_E - \overline{\tau^{\rm fin}}_E\right)}{2}\overline{\Delta u_1}A, \tag{22}$$

where $\overline{\Delta u_1}$ is the spatial average of Δu_1. Note that the difference between these two stress averages gives $\overline{\Delta\sigma}_E$. Hence $\overline{\tau^{\rm ini}}_E$ and $\overline{\tau^{\rm fin}}_E$ are the values to use as the initial and final stress averages in the energy-partitioning diagrams of the type shown in Fig. 3 (Noda & Lapusta 2012).

If $\Delta\sigma(x_1, x_3)$ is indeed uniform within the ruptured domain, then the three stress drop averages—$\overline{\Delta\sigma}_M$, $\overline{\Delta\sigma}_A$ and $\overline{\Delta\sigma}_E$—are all equal to each other, as follows from their expressions. In general, however, $\overline{\Delta\sigma}_E$ is not equal to either $\overline{\Delta\sigma}_M$ or $\overline{\Delta\sigma}_A$, and thus it is important to know how similar or different these stress drop measures are, for example, before using $\overline{\Delta\sigma}_M$ in place of $\overline{\Delta\sigma}_E$ for estimates of ΔW_0. We have proved that, for cases with heterogeneous stress drop, the energy-based stress drop average $\overline{\Delta\sigma}_E$ is always larger than the moment-based stress drop average $\overline{\Delta\sigma}_M$ (Appendix C).

In the following section, we assume heterogeneous slip distributions and compare those three measures of average stress drop.

3 COMPARISON OF THE AVERAGE STRESS DROP MEASURES FOR HETEROGENEOUS RUPTURES

3.1 Stochastic 2-D slip model

In our study, heterogeneous slip distributions are generated by randomizing an assumed characteristic slip distribution $\phi = (\phi_1, \phi_3)$ in a manner motivated by the 2-D stochastic model by Lavallée *et al.* (2006). Such approach is motivated by two considerations. First, it allows us to see the effects of heterogeneity on stress drops more clearly, by comparing the results to models with the uniform stress change over the ruptured domain, for which $\overline{\Delta\sigma}_M = \overline{\Delta\sigma}_A = \overline{\Delta\sigma}_E$. Secondly, it allows us to study the effect of the characteristic shape of the slip distribution, such as a triangular shape (e.g. Manighetti *et al.* 2005). The characteristic shape of slip distribution may result from the physics of the dynamic rupture process, making the slip distribution not fully stochastic. We assign the slip distribution as follows:

$$\Delta u_1(n_1, n_3) = C_n \phi_1(n_1, n_3) R(n_1, n_3),$$

$$\Delta u_2(n_1, n_3) = 0,$$

$$\Delta u_3(n_1, n_3) = C_n \phi_3(n_1, n_3), \tag{23}$$

where n_1 and n_3 are integer indices for the discrete point in the x_1 and x_3 directions, C_n is a normalization factor such that the ruptures studied here have unit potency and R is a filtered Gaussian random field with the mean and the standard deviation of 1 and χ, respectively. R can be written as

$$F[R - 1] = C_\chi H(k_{tr} - k) k^{-\frac{\nu+1}{2}} F[X], \tag{24}$$

where $F[\ ]$ represents discrete Fourier transformation, X is an uncorrelated random variable distributed over S, k is the length of a 2-D wavenumber vector, $\nu + 1$ is the decay rate in the power spectrum density of R with increasing k, H is the Heaviside step function, k_{tr} is the truncation wavenumber and C_χ is a constant which makes the standard deviation of the distribution equal to χ. As ν decreases and χ increases, the slip distribution becomes rougher in terms of its spectral structure and amplitude of fluctuation, respectively. Because M_{13} and M_{31} are the only non-zero components of the seismic moment tensor in this study, the spatial integration of $\Delta u_3(n_1, n_3)$ and ϕ_3 results in zero.

Lavallée *et al.* (2006) examined the finite fault inversion of strong ground motion data for 1994 Northridge earthquake (Liu & Archuleta 2000), and estimated the decay rate of the spectral power density of slip distribution ($\nu + 1$ if ϕ is uniform) as 1.74 and 2.05 for dip-slip and strike-slip components, respectively. They also examined several earthquakes using a 1-D model, and reported the decay rate from 1.78 to 2.71. Note that those values are such that the strain energy would diverge if all the wavenumbers were accounted for, and the truncation at a high wavenumber is required to deal with the problem in the framework of continuum mechanics. As discussed by Lavallée *et al.* (2006), this scaling behaviour is based on the assumption that the seismic process is lengthscale-independent for a wide but truncated range from the grain size to the rupture length (also see Andrews 1980). Note that the spectral structure of the slip distribution is modified from that implied by eq. (24) due to the multiplication by the characteristic shape ϕ. In this study, we investigate ν ranging from 0 to 2 (thus, $\nu + 1$ from 1 to 3) to randomize the uniform stress drop model. In our calculations, the characteristic length of the crack (the diameter of the circular crack or the shorter side of the rectangular crack) is set as a unit

length and discretized by 256 or 128 (in the cases with aspect ratio 16) gridpoints. The highest wavenumber k_{tr} is set as 128π.

We study cases with the characteristic slip function ϕ corresponding to uniform stress drop models for circular and rectangular cracks of different aspect ratios, and several other slip shapes. Out of the cases considered, ϕ_3 is non-zero only for the cases with uniform stress drop in rectangular cracks. If we choose ϕ based on the uniform stress drop model, stress drop distribution $\Delta\sigma$ becomes uniform inside Σ at $\chi = 0$ and hence the three average stress drop measures are equal to each other for $\chi = 0$. As χ increases, $\Delta\sigma$ is expected to be more and more heterogeneous.

Lavallée *et al.* (2006) reported that the probability distribution of slip in a single event is better explained by Lévy α-stable distribution than Gaussian or Cauchy distributions, both of which are special cases of Lévy α-stable distribution. In this study, however, we employ Gaussian distribution for the random variable X for simplicity. Liu-Zeng *et al.* (2005) studied the length of 1-D ruptures generated using a stochastic model with Gaussian distribution similar to the one used in this work. Gaussian distribution has two parameters (mean and variance) so that the randomness of X is controlled by a single parameter χ, while Lévy α-stable distribution has four parameters (the characteristic exponent, skewness, scale and location), and they cause additional complexity. It would be important to investigate the effect of other probability distributions (e.g. Cauchy and Lévy) in future studies.

Manighetti *et al.* (2005) examined not only results of finite source inversions of seismological and geodetic observations, but also geologically measured surface rupture profiles, and concluded that the slip distribution is typically triangular with various skewness. The triangular slip distributions can be generated by realizations of different probability distribution functions, but in this study we instead randomize a characteristic tapering functions ϕ, including a triangular-shaped ϕ. By doing so, we can examine the effect on the average stress drop measures of not only the roughness (i.e. spectral decay power and amplitude of the random field), but also the characteristic shape of slip distributions. For each selection of ϕ, ν and χ, we have analysed 100 random cases.

It should be noted that given the non-uniqueness of the geophysical inversion problems and smoothness constraint (e.g. Minson 2010), it is somewhat arguable how well those slip distributions, especially their short wavelength features, are constrained. We are not intending to support or disqualify the proposed statistical model of the slip distribution, but take the randomization as a way of producing examples, a series of distributions with controlled roughness. To what extent we can constrain the slip distribution is an important future task in observational seismology.

$\Delta\sigma$ is calculated using the spectral boundary integral equation method (BIEM) after embedding the slip distribution in a domain four times larger (in length) than the ruptured domain. This is to prevent the effect of periodic replications on one another. We use the standard elastostatic formulae in the spectral domain (e.g. Lapusta & Liu 2009)

$$\begin{bmatrix} F[\Delta\sigma_1] \\ F[\Delta\sigma_3] \end{bmatrix} = \frac{\mu}{2k} \begin{bmatrix} k_1^2/(1-\nu_p) + k_3^2 & k_1 k_3 \nu_p/(1-\nu_p) \\ k_1 k_3 \nu_p/(1-\nu_p) & k_1^2 + k_3^2/(1-\nu_p) \end{bmatrix}$$
$$\times \begin{bmatrix} F[\Delta u_1] \\ F[\Delta u_3] \end{bmatrix}, \tag{25}$$

where ν_p is the Poisson's ratio which is assumed to be 1/4. Note that we shall present the results normalized by $\overline{\Delta\sigma}_M$ so that the value of shear modulus μ is not important in this study.

3.2 Effect of the roughness of the random field

In this section, effects of randomization of the uniform stress drop models are discussed. Such models have elliptical ϕ_1 for a circular crack. Figs 4(a) and (b) show examples of the distributions of Δu_1 and $\Delta\sigma_1/\overline{\Delta\sigma}_M$, respectively, for different randomization parameters ν and χ. The number in each panel indicates the maximum value of the field plotted. The left-most column ($\chi = 0$) corresponds to cases without randomization. Note that the discretely sampled elliptical function for ϕ produces a numerical error in $\Delta\sigma$ which is significant near the crack tip. This is why the maximum value of $\Delta\sigma_1/\overline{\Delta\sigma}_M$ is not equal to one in the left-most column. In the case of uniform stress drop, we can test the effect of this numerical error

and find that it affects $\overline{\Delta\sigma}_A/\overline{\Delta\sigma}_M$ by 2 per cent, and $\overline{\Delta\sigma}_E/\overline{\Delta\sigma}_M$ by 4 permille. Such errors are negligibly small compared with the differences between the stress drop estimates discussed in this study.

With increasing χ, the variance in Δu_1 increases and we sometimes obtain locally negative slip which may not be realistic. This is why we investigate the value of χ only up to 0.5.

The heterogeneity in slip strongly affects the local distribution of stress drop $\Delta\sigma$, as can be expected. The amplitude of variations in $\Delta\sigma_1$ increases as χ increases and ν decreases. In the most rough case shown (the bottom-right panel in Fig. 4), the maximum value of $\Delta\sigma_1/\overline{\Delta\sigma}_M$ is more than 100. If such heterogeneity is realistic, the seismologically estimated average stress drop of 3 MPa would
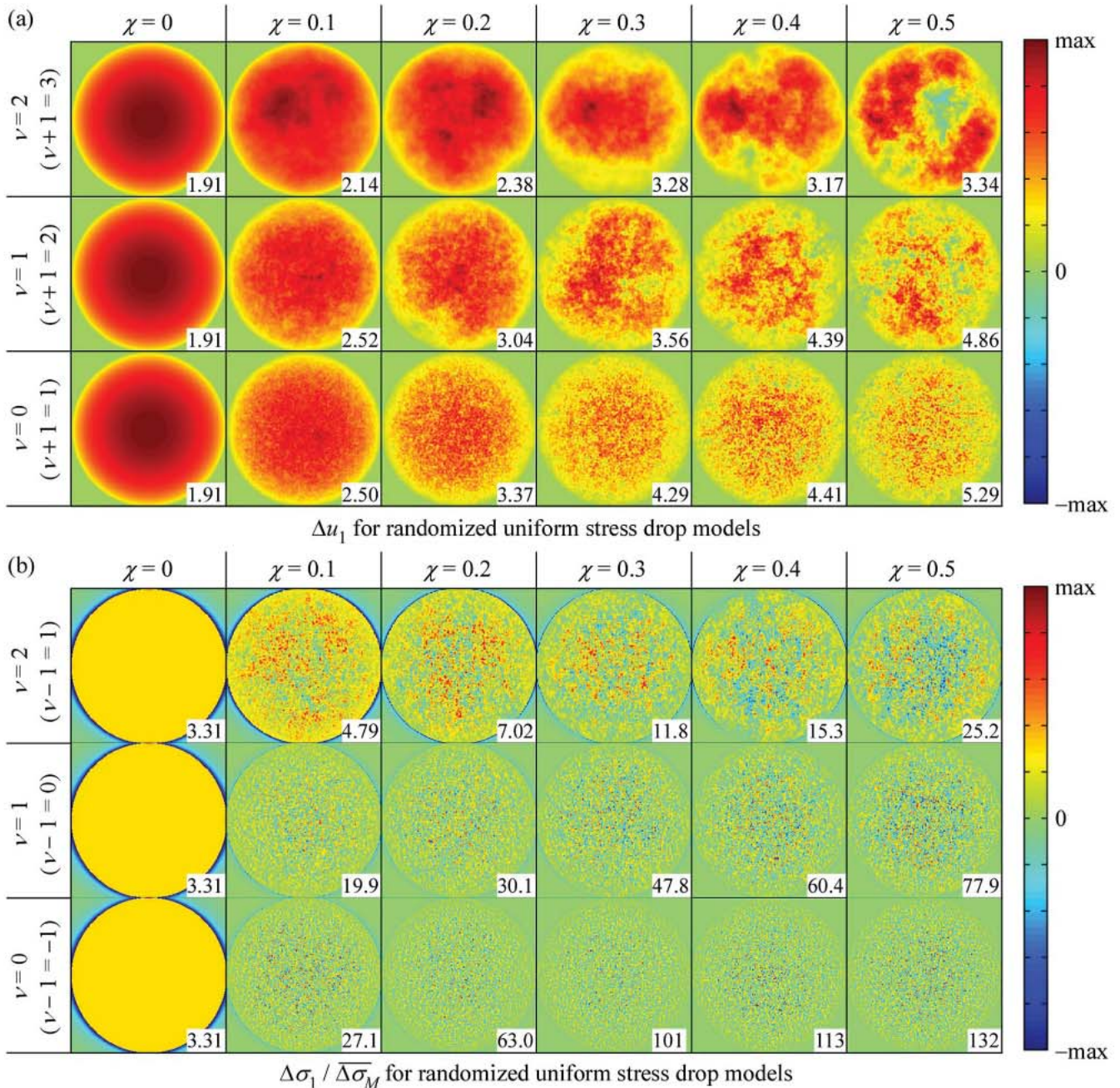

Δu_1 for randomized uniform stress drop models

$\Delta\sigma_1 / \overline{\Delta\sigma}_M$ for randomized uniform stress drop models

Figure 4. Examples of distributions of (a) Δu_1 and (b) $\Delta\sigma_1/\overline{\Delta\sigma}_M$ for models based on the circular crack model with uniform stress drop (i.e. elliptical ϕ_1). Since the spectrum decay rate of the stress drop distribution is smaller by 1 than that of the slip distribution, $\nu - 1$ is indicated in (b). The number at the bottom right of each panel indicates the maximum value of the plotted field. The diameter of the circle and the potency are normalized to 1.
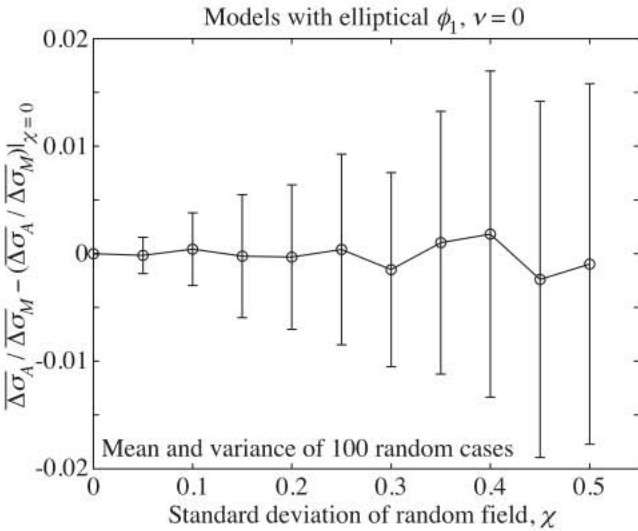
Models with elliptical ϕ_1, $\nu = 0$

Figure 5. Mean and variance of $\overline{\Delta\sigma}_A/\overline{\Delta\sigma}_M$ relative to the case with uniform stress drop ($\chi = 0$). Models based on elliptical ϕ_1 with $\nu = 0$ are shown here. Examples are shown in the bottom row in Fig. 4. Randomization affects $\overline{\Delta\sigma}_A$ by at most 2 per cent (for one standard deviation) in all cases studied, although the local variation in $\Delta\sigma_1$ is much larger (Fig. 4 b).

correspond to the amplitude of local stress change $\Delta\sigma_1$ of the order of 300 MPa. The local stress drop can also be negative. The possibility of negative local stress drop within areas of positive slip has been recently demonstrated by earthquake sequence simulations (Noda & Lapusta 2010a). The pattern of positive and negative stress drops has also been inferred from observations (e.g. Bouchon 1997).

At the same time, we find that the spatially averaged stress drop $\overline{\Delta\sigma}_A$ is not much affected by the randomization. Fig. 5 shows the variation in $\overline{\Delta\sigma}_A$ as a function of χ for the cases with $\nu = 0$. Even when the local fluctuation of $\Delta\sigma_1/\overline{\Delta\sigma}_M$ is larger than two orders of magnitude, the variation in $\overline{\Delta\sigma}_A$ is less than 0.02 of $\overline{\Delta\sigma}_M$. This observation suggests that $\overline{\Delta\sigma}_A$ is mainly controlled by the overall shape of slip distribution ϕ. This issue is further discussed in the next section.

The energy-based stress drop $\overline{\Delta\sigma}_E$ increases as the slip distribution becomes rougher both in terms of the amplitude and the spectral structure. Fig. 6 shows the contour lines of $\overline{\Delta\sigma}_E/\overline{\Delta\sigma}_M$. Note that
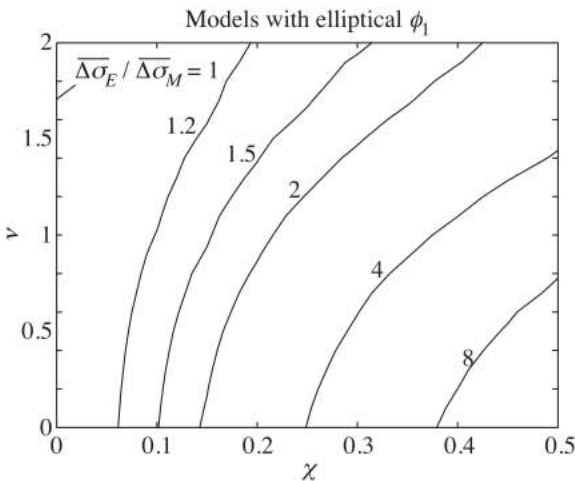
the horizontal and vertical axes correspond to those in Fig. 4. We find that randomization always increases $\overline{\Delta\sigma}_E/\overline{\Delta\sigma}_M$, which can also be proven theoretically (Appendix C). This means that if one uses seismologically estimated stress drop $\overline{\Delta\sigma}_M$ in eq. (18), the partial strain energy change ΔW_0 is always underestimated.

All conclusions obtained in this section for circular ruptures hold for the rectangular cases as well. The details are given in Appendix B2.

3.3 Effect of overall shape of slip distribution

The heterogeneous slip distributions are built in eq. (23) by randomizing the characteristic slip distribution ϕ. The expected form of ϕ varies depending on the physics and dynamics of rupture process. If the rupture is crack-like and expanding in a self-similar manner, the characteristic shape could be elliptical or a more concentrated variant of that due to the inward propagation of the stopping phase. If the rupture is pulse-like, then the characteristic slip shape may be increasing with the propagation distance for a growing pulse or stay constant for a steady pulse. Different arrest mechanisms would result in different tapering of the shape at the edge of the rupture. Based on a number of observed slip distributions for natural earthquakes, Manighetti *et al.* (2005) concluded that the slip distributions are typically triangular with various skewness. Böse & Heaton (2010) used the idea of an average slip shape to construct a procedure for predicting the final length of ongoing rupture. They followed the study of Ward (2004) in assuming that the mean slip function is represented by a function which is derived from a restricted random walk process.

Fig. 7 shows the effect of ϕ on $\overline{\Delta\sigma}_E/\overline{\Delta\sigma}_M$ and $\overline{\Delta\sigma}_A/\overline{\Delta\sigma}_M$ for several simple shapes. We have considered elliptical, smoothed boxcar, trapezoidal, triangular and sinusoidal radial distributions for ϕ_1, keeping $\phi_3 = 0$. Cases with $\nu = 1$ and $\chi = 0.3$ are shown as well as cases without randomization (i.e. $\chi = 0$). Note that the ruptured domain Σ is a circle with the unit diameter for all those cases. For the smoothed boxcar function, we use

$$\phi_1 = \begin{cases} 1, & r' < 0.4 \\ \frac{1}{2}\left[1 + \tanh\left(\frac{0.1}{r'-0.5} + \frac{0.1}{r'-0.4}\right)\right], & 0.4 \le r' < 0.5 \,, \quad (26) \\ 0, & 0.5 \le r' \end{cases}$$

where r' is the radial coordinate measured from the centre of the circular crack.

If ϕ is different from the one for the uniform stress drop model, then $\overline{\Delta\sigma}_A$ as well as $\overline{\Delta\sigma}_E$, differs from $\overline{\Delta\sigma}_M$, even without randomization (Fig. 7, crosses and pluses in lower panels). The difference for the cases studied is within a factor of two, which is relatively small compared to the uncertainties in the seismological stress drop estimates (Allmann & Shearer 2009). Randomization and introduction of small scale heterogeneity increases $\overline{\Delta\sigma}_E$, but causes little additional changes in $\overline{\Delta\sigma}_A$. When the slip distribution is tapered more smoothly than that for the uniform stress drop, the stress concentration (which is outside Σ in the uniform stress drop models) partially occurs inside Σ. This creates a region of negative $\Delta\sigma_1$ inside Σ and affects the area-averaged stress drop measure $\overline{\Delta\sigma}_A$. Therefore, how a rupture is arrested is important for the value of $\overline{\Delta\sigma}_A$.

In all cases studied, we find $\overline{\Delta\sigma}_E > \overline{\Delta\sigma}_M$; the theoretical proof of this relation is given in Appendix C. The relation $\overline{\Delta\sigma}_M > \overline{\Delta\sigma}_A$ holds for most cases but not always. For example, in cases for randomized uniform stress drop models described in the last section, $\overline{\Delta\sigma}_M$ is smaller than $\overline{\Delta\sigma}_A$ in about 50 per cent of the random cases,
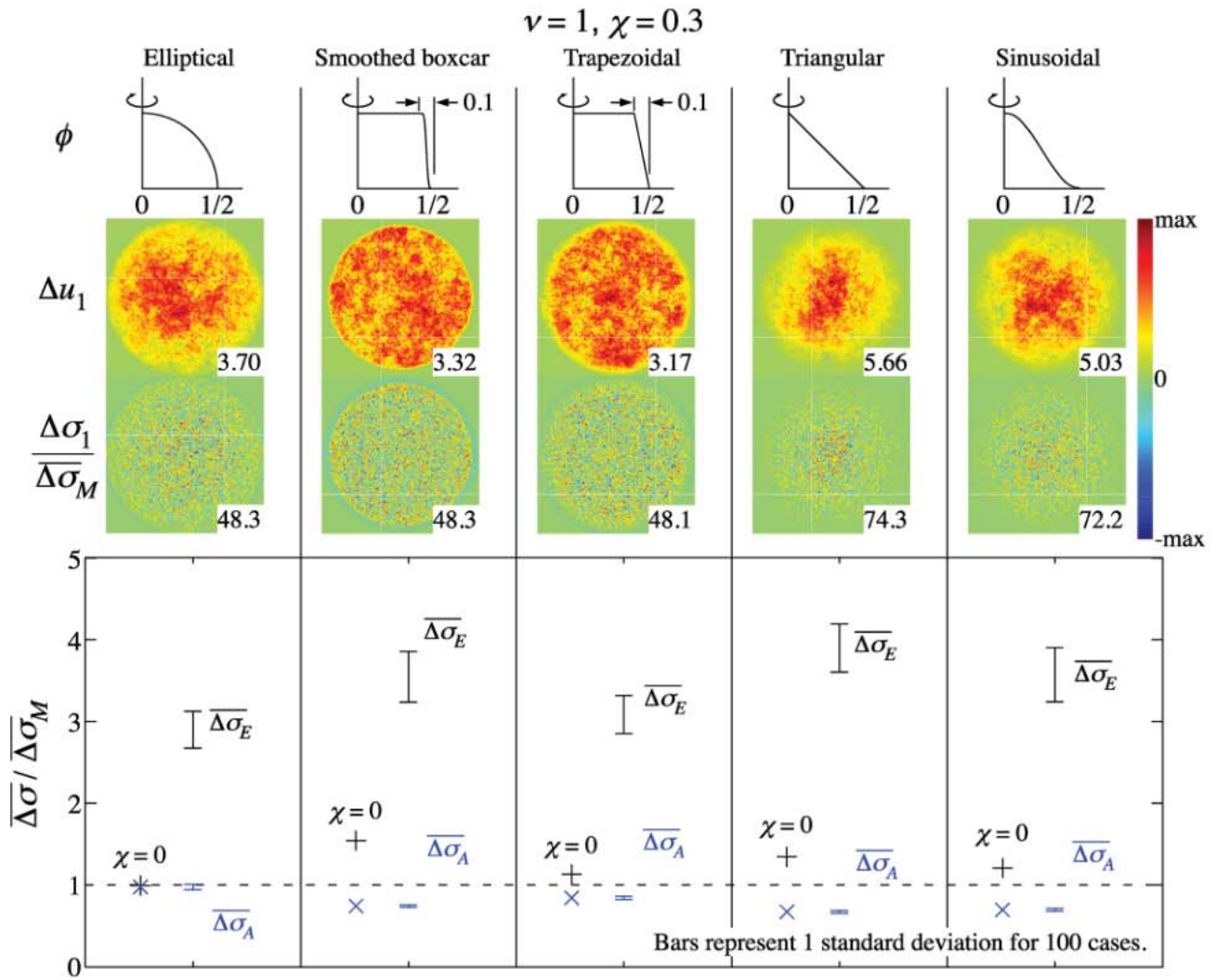
Models with elliptical ϕ_1

Figure 6. Contours of $\overline{\Delta\sigma}_E/\overline{\Delta\sigma}_M$ averaged for 100 random models based on elliptical ϕ_1. The horizontal and vertical axes correspond to those in Fig. 4.

Figure 7. Effect of the characteristic shape ϕ on $\overline{\Delta\sigma}_E/\overline{\Delta\sigma}_M$ and $\overline{\Delta\sigma}_A/\overline{\Delta\sigma}_M$. Top row: ϕ as a function of radius from the centre of the rupture. Middle row: examples of distributions of Δu_1 and $\Delta\sigma_1/\overline{\Delta\sigma}_M$ with $\nu = 1$ and $\chi = 0.3$. Bottom row: values of $\overline{\Delta\sigma}_E/\overline{\Delta\sigma}_M$ (black) and $\overline{\Delta\sigma}_A/\overline{\Delta\sigma}_M$ (blue). Crosses and pluses represent the cases without randomization (i.e. $\chi = 0$).

so that the average of $\overline{\Delta\sigma}_A/\overline{\Delta\sigma}_M$ is approximately one. In order to have $\overline{\Delta\sigma}_M < \overline{\Delta\sigma}_A$, we need concentration of large stress drop near the crack tip where E_1^{12} is smaller than in the central region(recall that $\overline{\Delta\sigma}_M$ is the average of $\Delta\sigma_1$ using E_1^{12} as a weight function). In the extreme case with Δu_1 being a boxcar function, $\overline{\Delta\sigma}_A/\overline{\Delta\sigma}_M$ would become infinitely large because of the singularity at the crack tip.

4 IMPLICATIONS FOR EARTHQUAKE SOURCE CHARACTERISTICS

4.1 Energy partitioning and constraints on shear stress evolution

In this section, we discuss the consequences of our findings on systematic differences between $\overline{\Delta\sigma}_E$ and $\overline{\Delta\sigma}_M$ for the values of radiation ratio obtained by Venkataraman & Kanamori (2004) and then examine the implications of those values for shear stress evolution during earthquakes.

Venkataraman & Kanamori (2004) computed the radiation ratio $\eta_R = E_R/\Delta W_0$ for large earthquakes ($M_w > 6.5$) and found that

most of the earthquakes examined by them, except for tsunami earthquakes and a deep 1994 Bolivia earthquake, had η_R ranging from 0.25 to 1. Their calculations used the seismologically estimated stress drops ($\overline{\Delta\sigma}_M$). Note that η_R can be expressed as

$$\eta_R = E_R/\Delta W_0 = \frac{2\mu E_R}{\overline{\Delta\sigma}_E M_0}. \qquad (27)$$

Our finding that the energy-based $\overline{\Delta\sigma}_E$ that enters eq. (27) is always larger than the moment-based $\overline{\Delta\sigma}_M$ (Section 4.1, appendix C) suggests that the radiation ratios η_R of large earthquakes may be even smaller than what was estimated by Venkataraman & Kanamori (2004), and perhaps much smaller if the stress change distribution is quite heterogeneous. More significant heterogeneity in slip distributions would lead to larger $\overline{\Delta\sigma}_E$ in comparison to $\overline{\Delta\sigma}_M$, hence to more significant underestimation of the partial strain energy change ΔW_0, and thus to more significant overestimation of η_R. (Note that small-scale slip heterogeneity is not resolvable by finite fault inversions.)

Note that any differences that exist between $\overline{\Delta\sigma}_E$ and $\overline{\Delta\sigma}_M$ because of the theoretically different averaging inherent in these quantities are in addition to any existing uncertainties in determining

$\overline{\Delta\sigma}_M$ from seismic observations (Pavic *et al.* 2000; Allmann & Shearer 2009). For example, if the uncertainty due to determining $\overline{\Delta\sigma}_M$ is a factor of up to 3 and the potential difference between $\overline{\Delta\sigma}_E$ and $\overline{\Delta\sigma}_M$ is a factor of up to 8, then the combined uncertainty factor in the energy arguments would be up to 24, which is more than an order of magnitude.

The conclusion of Venkataraman & Kanamori (2004) that radiation ratio η_R is typically smaller than 1 for typical large natural earthquakes—which is further strengthened by our results—can be used to restrict the range of potential scenarios for evolution of shear stress with slip during seismic events. While $\eta_R < 1$ is true for the simplified diagram of Fig. 3 by construction, $\eta_R > 1$ is theoretically allowed. This is because more energy than ΔW_0 can be available for radiation, if the dissipation on the fault is smaller than E_F (Section 1), as discussed in more detail in the following.

The radiated energy can be written as (Kostrov & Das 1988)

$$E_R = \frac{1}{2}\int_\Sigma (\boldsymbol{\tau}^{\mathrm{ini}} - \boldsymbol{\tau}^{\mathrm{fin}})\cdot\Delta\boldsymbol{u}\,\mathrm{d}S + \int_0^{t^{\mathrm{fin}}}\mathrm{d}t\int_\Sigma \frac{\mathrm{d}\boldsymbol{\tau}}{\mathrm{d}t}\cdot\boldsymbol{\delta}\,\mathrm{d}S$$

$$\approx \frac{1}{2}\int_\Sigma (\tau_1^{\mathrm{ini}} - \tau_1^{\mathrm{fin}})\Delta u_1\,\mathrm{d}S + \int_0^{t^{\mathrm{fin}}}\mathrm{d}t\int_\Sigma \frac{\mathrm{d}\tau_1}{\mathrm{d}t}\delta_1\,\mathrm{d}S, \qquad (28)$$

where t^{fin} is the time when all wave-mediated processes are finished, and τ and δ are shear traction and slip vectors on the fault during the dynamic rupture process. In many cases, the slip vector is dominated by the component in the overall slip direction (e.g. Noda & Lapusta 2012) and we shall neglect the contribution from the other component in the following discussion. In eq. (28), the energy of new surface creation is absorbed in the frictional dissipation, which also includes the potential increased dissipation at the rupture tip analogous to fracture energy of singular crack theory. Multiplying both sides by the factor that converts E_R into η_R (eq. 27), we obtain

$$\eta_R = 1 + \frac{2\mu}{\overline{\Delta\sigma}_E M_0}\int_0^{t^{\mathrm{fin}}}\mathrm{d}t\int_\Sigma \frac{\mathrm{d}\tau_1}{\mathrm{d}t}\delta_1\,\mathrm{d}S. \qquad (29)$$

From eq. (29), whether η_R is larger or smaller than one depends on the sign of the integral, and hence on the sign of the time derivative of the local shear stress evolution, $\mathrm{d}\tau_1/\mathrm{d}t$, if one makes a reasonable and general assumption that slip is positive. For example, if $\mathrm{d}\tau_1/\mathrm{d}t \le 0$ for all non-negligible slips, then $\eta_R \le 1$. A particular case of such behaviour is shown in the conceptual diagram of Fig. 3.

Of course, the sign of $\mathrm{d}\tau_1/\mathrm{d}t$ may vary during dynamic rupture process, potentially resulting in $\eta_R > 1$. Recent experiments (e.g. Fukuyama & Mizoguchi 2009; Sone & Shimamoto 2009) suggested that fault resistance with slip may drop substantially to near-zero values and then substantially recover (restrengthen) as slip rates decrease at the end of the local slip. Such behaviour is sometimes advocated as the basis for pulse-like ruptures (e.g. Heaton 1990). Fig. 8(a) schematically reproduces one of the experimental curves (based on fig. 4 a in Sone & Shimamoto 2009). Since the sign of $\mathrm{d}\tau_1/\mathrm{d}t$ varies during such behaviour and, in particular, is positive at the end of slip when the values of slip are largest, the sign of the integral in eq. (29), and hence the relation of η_R to 1, is no longer clear for such scenarios.

Before analysing the energy balance for cases with variable $\mathrm{d}\tau_1/\mathrm{d}t$ in more detail, using the scenarios of Fig. 8 as examples, let us briefly explain what the diagrams of Fig. 8 represent in terms of dynamic rupture process. Fig. 9 illustrates different stress quantities marked in Fig. 8. The shear stress on the fault is treated as a scalar quantity in Fig. 9 for simplicity. As the dynamic rupture propagates on the fault (Fig. 9a), the shear stress at a point varies (Figs 9b and c). Right before the dynamic rupture, the fault has prestress (or initial stress) τ^{ini}. Slip initiates at a higher value of stress reached through stress concentration at the rupture front; we denote this stress value by τ_{beg}. The stress level at the termination of slip at a point along the fault is denoted by τ_{ter}. The final stress τ^{fin}, after the passage of all waves, can be readjusted by the waves to be either higher or smaller than τ_{ter}. The values of these stress quantities averaged over the fault based on energy considerations are denoted by adding overlines and, for two of them, subscripts E, and marked in Figs 8 and 9(d). The average dissipative stress curves (solid lines in Figs 8 and 9d) are constructed so that (i) the area under the curve gives energy dissipation per unit fault area and (ii) the characteristic local features of the stress-slip behaviour are attempted to be preserved in the averaging. The averaging procedure that achieves these goals is described in Noda & Lapusta (2012). The ends of the virtual work rate, $\overline{\tau^{\mathrm{ini}}}_E$ and $\overline{\tau^{\mathrm{fin}}}_E$, are given by eq. (20) and (21).

It should be emphasized that the variation of shear stress at the fault points that have arrested—due to wave-mediated stress transfers from fault points that are still slipping—contributes to the integral in eq. (29), and hence such variation plays an important role in determining whether η_R exceeds 1 or not. On the other hand, the shear stress change before beginning of significant slip (e.g. stress concentration in front of rupture tip) does not contribute to the integral and thus does not affect the sign of $\eta_R - 1$. Hence, in different scenarios of stress versus slip behaviour, the sign of $\eta_R - 1$ can be changed by varying the final stress $\overline{\tau^{\mathrm{fin}}}_E$ but not the initial stress $\overline{\tau^{\mathrm{ini}}}_E$. However, for a given final stress $\overline{\tau^{\mathrm{fin}}}_E$, the initial stress $\overline{\tau^{\mathrm{ini}}}_E$ is constrained by other physical considerations, such as the requirements of the positive stress drop $\overline{\Delta\sigma}_E$ and the positive radiated energy E_R.

In the experimentally-motivated scenario of Fig. 8(a), the radiation ratio η_R is larger than 1. The partial strain energy ΔW_0 is given by the striped triangle, and it is clearly smaller than the radiated energy E_R, given by the difference between the grey areas marked with '+' and '−'. In terms of the integral of eq. (29), what we would find is that the positive contribution from the increasing dissipative stress at large slips overwhelms the negative contributions during fault weakening.

The scenario of Fig. 8(a) has the following characteristic features. The average prestress $\overline{\tau^{\mathrm{ini}}}_E$ and final stress $\overline{\tau^{\mathrm{fin}}}_E$ are close to each other, in the sense that their difference $\overline{\Delta\sigma}_E$ is much smaller than their magnitude. However, the typical dynamic resistance is substantially lower than either $\overline{\tau^{\mathrm{ini}}}_E$ or $\overline{\tau^{\mathrm{fin}}}_E$, representing significant dynamic weakening (and then restrengthening), and hence having substantial undershoot. To understand why such 'substantially weakening-then-substantially strenthening' scenario leads to $\eta_R > 1$, let us consider the idealized version of it (Fig. 8b), in which the dynamic resistance is constant at $\overline{\tau_d}$ and the transitions between the initial stress $\overline{\tau^{\mathrm{ini}}}_E$, the peak stress $\overline{\tau_p}$, the dynamic resistance $\overline{\tau_d}$ and the final stress $\overline{\tau^{\mathrm{fin}}}_E$ are achieved with negligible slip. Then ΔW_0 is represented by the striped triangle in Fig. 8(b) and E_R is given by the much larger grey area, resulting in $\eta_R \gg 1$. In terms of formulae, we get

$$\eta_R = E_R/\Delta W_0 = \frac{(\overline{\tau^{\mathrm{ini}}}_E + \overline{\tau^{\mathrm{fin}}}_E)\overline{\Delta u_1}/2 - \overline{\tau_d}\,\overline{\Delta u_1}}{\overline{\Delta\sigma}_E\overline{\Delta u_1}/2}$$

$$= \frac{(\overline{\tau^{\mathrm{ini}}}_E - \overline{\tau_d}) + (\overline{\tau^{\mathrm{fin}}}_E - \overline{\tau_d})}{\overline{\Delta\sigma}_E} \gg 1, \qquad (30)$$
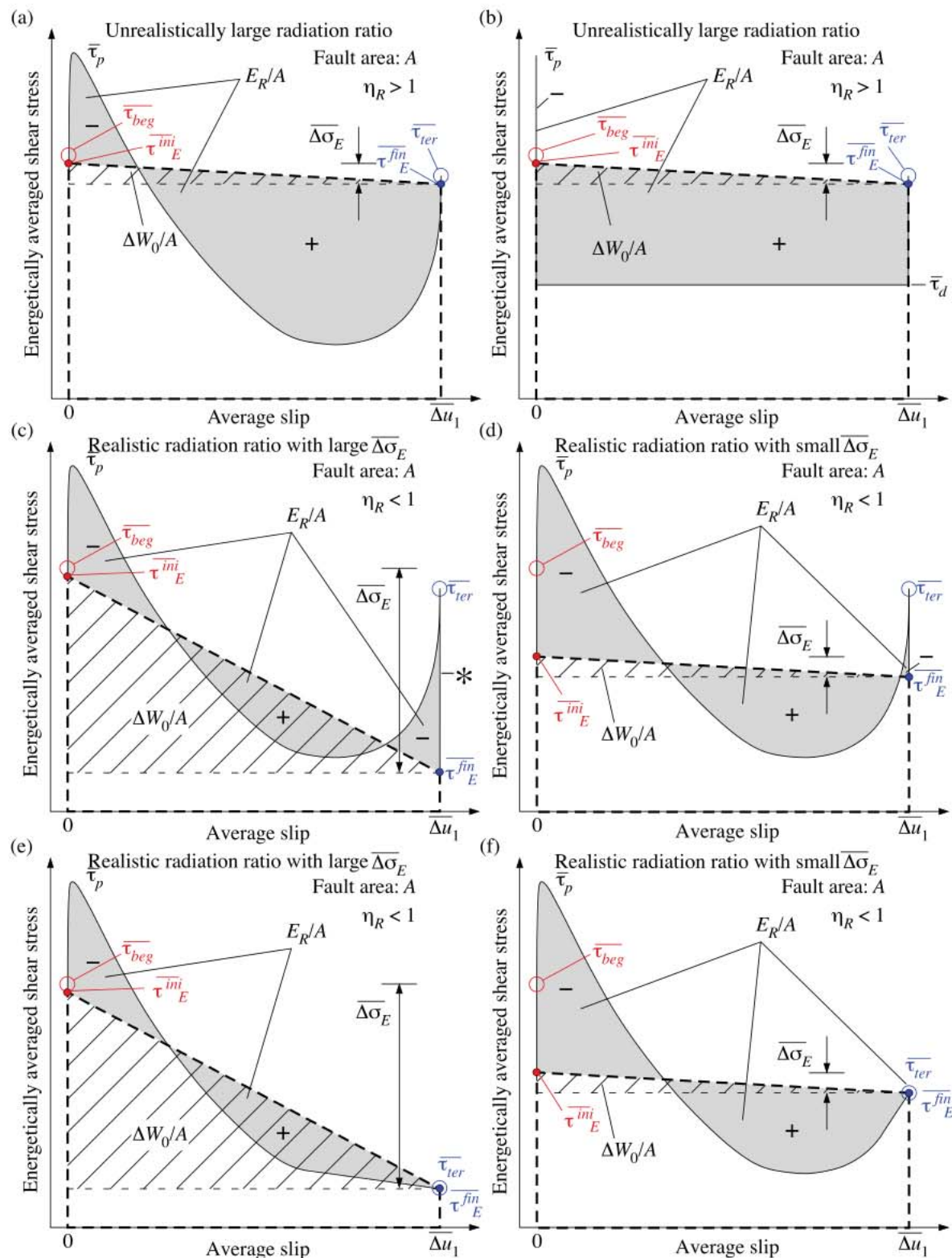
Figure 8. Schematic diagrams showing energy partitioning in different stress evolution scenarios. (a) Scenario based on laboratory experiments (Sone & Shimamoto 2009) which leads to $\eta_R \gg 1$. It is characterized by a small difference between the initial and final stresses compared to their difference with the typical dynamic frictional resistance. This leads to significant weakening at the beginning of slip followed by significant restrengthening at the end of slip. (b) The idealized version of such scenario, simplified by assuming negligible dissipation above the constant dynamic frictional resistance. (c)–(d) Scenarios with η_R smaller than unity obtained from the case of panel a by reducing only $\overline{\tau^{fin}}_E$ (panel c) or both $\overline{\tau^{ini}}_E$ and $\overline{\tau^{fin}}_E$ (panel d). The two cases result in different moment-based stress drop. (e)–(f) Streamlined versions of scenarios (c)–(d), in which the stress behaviour at the end of slip is simplified. The value of $\overline{\tau^{fin}}_E$ for $\eta_R = 1$ is indicated by a star in panel c.
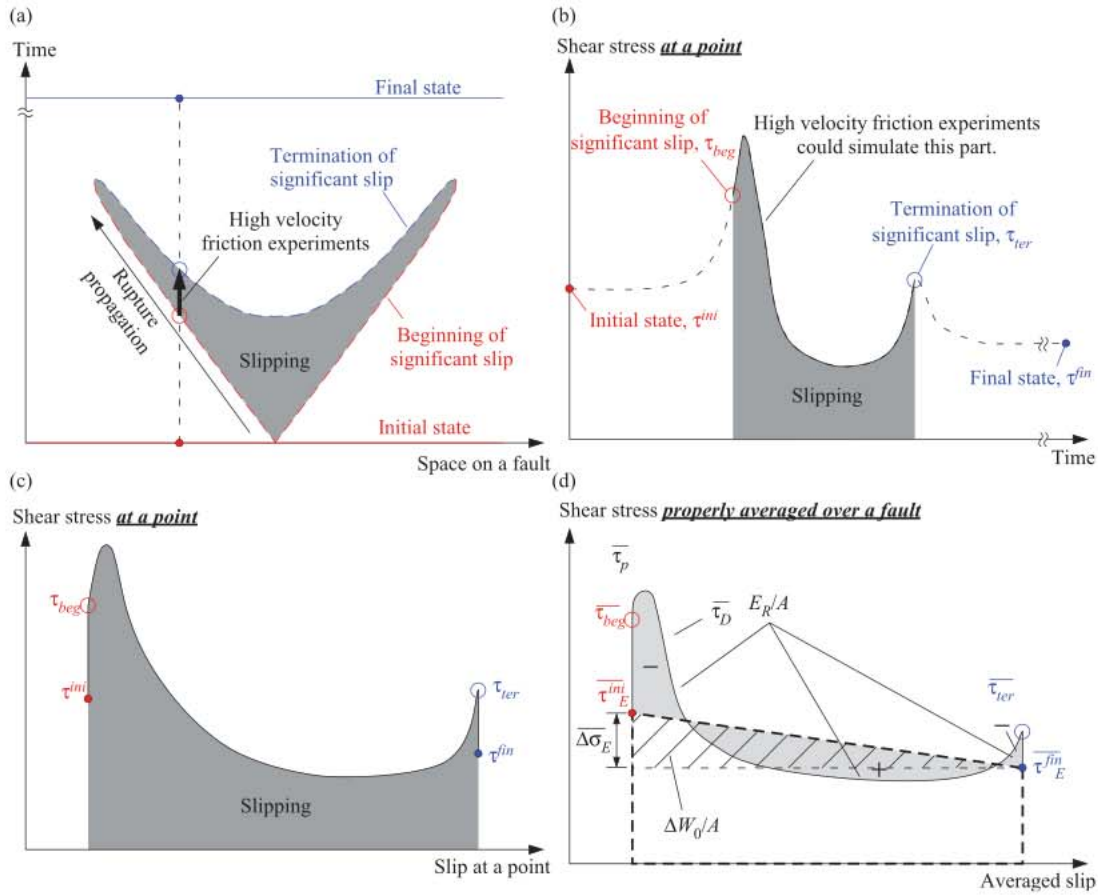
Figure 9. Schematic diagrams showing the dynamic rupture process and several stress levels important for the discussion of energy partitioning. (a) A dynamic rupture process in the space–time domain. (b) Shear stress as a function of time at a point on the fault. In general, there are differences between the initial stress state and the stress at the beginning of significant slip and between the final stress state and the stress at the termination of significant slip. (c) Shear stress as a function of slip at a point on the fault. (d) Schematic fault-averaged evolution of the shear stress with slip which differs, in general, from the one at each particular fault location.

since $(\overline{\tau^{\text{ini}}}_E - \overline{\tau_{\text{d}}}) \gg \overline{\Delta\sigma}_E$ and $(\overline{\tau^{\text{fin}}}_E - \overline{\tau_{\text{d}}}) \gg \overline{\Delta\sigma}_E$ by construction of the scenario. Hence, the scenario in Fig. 8(b) (as well as 8a) contradicts the observations on radiation ratio.

Note that the behaviour illustrated in Figs 8(a) and (b) can occur on parts of the fault (i.e. for local shear stress as a function of local slip) without contradicting the observations on the radiation ratio, as long as such behaviour is compensated for by the behaviours at other fault locations, so that the average dissipation behaviour is different.

One can adjust the experimentally motivated scenario in Fig. 8(a) to result in η_R which is smaller than 1 without changing the overall shape, by adjusting the initial and final stresses $\overline{\tau^{\text{ini}}}_E$ and $\overline{\tau^{\text{fin}}}_E$. Changing only $\overline{\tau^{\text{ini}}}_E$ (while keeping the same $\overline{\tau^{\text{fin}}}$) changes η_R but not the sign of $\eta_R - 1$. This can be easily seen from the energy balance. Writing $\Delta W = E_R + D$, where D is the total dissipation (including the increased dissipation at the rupture tip) and subtracting from both sides the dissipation $E_F = \overline{\tau^{\text{fin}}}_E \overline{\Delta u} A$ that would have occurred if slip were accumulated with the resistance equal to the final stress $\overline{\tau^{\text{fin}}}_E$, we obtain

$$\Delta W_0 = E_R + (D - E_F) = E_R + (D - \overline{\tau^{\text{fin}}}_E \overline{\Delta u}_1 A), \tag{31}$$

$$\eta_R = 1 - (D - \overline{\tau^{\text{fin}}}_E \overline{\Delta u}_1 A)/\Delta W_0. \tag{32}$$

From eq. (32), we clearly see that the sign of the second term depends on the sign of the difference between the actual dissipation D and the dissipation E_F that would have occurred if the stress during the entire rupture would be equal to the final stress. This difference does not depend on $\overline{\tau^{\text{ini}}}_E$, but clearly does depend on $\overline{\tau^{\text{fin}}}_E$. The difference is trivially positive (and hence $\eta_R <$ 1) for scenarios in which the dissipative stress is always above the final stress $\overline{\tau^{\text{fin}}}_E$ (e.g. scenarios with overshoot). Eq. (32) can also be obtained from eq. (29) by integrating the second term by parts.

Hence, to achieve $\eta_R < 1$ for the scenarios of Figs 8(a) and (b), we need to decrease the final stress $\overline{\tau^{\text{fin}}}_E$ (Fig. 8c). In the idealized scenario of Fig. 8(b), the final stress $\overline{\tau^{\text{fin}}}_E$ has to become smaller than the dynamic resistance $\overline{\tau_{\text{d}}}$, leading to overshoot, since $\overline{\tau^{\text{fin}}}_E = \overline{\tau_{\text{d}}}$ leads to $\eta_R = 1$ in eq. (30). However, in the more general scenario of Fig. 8(a), the additional dissipation makes it possible to achieve $\eta_R < 1$ without overshoot or with a mild undershoot. Fig. 8(c) shows a scenario where the radiated energy E_R is near-zero, and any further decrease in $\overline{\tau^{\text{fin}}}_E$ would not be physical (as it would result in negative E_R). The position of $\overline{\tau^{\text{fin}}}_E$ that would be the highest for the condition $\eta_R < 1$ to hold is indicated by a star in Fig. 8(c).

The decrease in $\overline{\tau^{\text{fin}}}_E$ would increase the difference between $\overline{\tau^{\text{ini}}}_E$ and $\overline{\tau^{\text{fin}}}_E$, and hence lead to larger values of energy-based stress

drop $\overline{\Delta\sigma}_E$. If the stress drop is relatively homogeneous, so that $\overline{\Delta\sigma}_E$ is comparable to $\overline{\Delta\sigma}_M$, then the stress drops may become too large compared to the observed values of the order of 1–10 MPa for large events (e.g. Kanamori & Anderson 1975). For example, if the shear stress on the fault is determined by ambient normal stress and hydrostatic pore fluid pressure, times the friction coefficient which decreases from typical peak values of 0.7 to low dynamic values of 0.1 due to high-velocity weakening, then the strength drop (the difference between the maximum and minimum of the dissipation rate) is of the order of 100 MPa. To avoid issues with stress drop, there are two possibilities. Either the slip distribution has to be relatively heterogeneous, so that $\overline{\Delta\sigma}_E$ is much larger than $\overline{\Delta\sigma}_M$. Or $\overline{\Delta\sigma}_E$ is in fact of the order of 1–10 MPa, pointing to low overall strength and hence strength drop, for example, due to ambient fluid overpressure.

Scenarios similar to Figs 8(a) and (b) can achieve both $\eta_R < 1$ and smaller $\overline{\Delta\sigma}_E$ than in Fig. 8(c) by lowering both $\overline{\tau^{\text{ini}}}_E$ and $\overline{\tau^{\text{fin}}}_E$ (Fig. 8d). In this scenario, the prestress $\overline{\tau^{\text{ini}}}_E$ moves further away from the peak stress $\overline{\tau}_p$, resulting in fault operation under lower overall shear stress than $\overline{\tau}_p$ that may be comparable to the static strength. Such scenarios have been shown to favour pulse-like ruptures (e.g. Perrin *et al.* 1995; Zheng & Rice 1998; Noda *et al.* 2009).

Note that while the sign of $\eta_R - 1$ does not depend on the initial stress $\overline{\tau^{\text{ini}}}_E$, the energy partitioning overall does. The upper bound for $\overline{\tau^{\text{ini}}}_E$ is given by a situation in which the fault is uniformly loaded to just below τ_{beg} (at which slip would start). As $\overline{\tau^{\text{ini}}}_E$ decreases from that upper bound, assuming the same $\overline{\tau^{\text{fin}}}_E$, ΔW_0 (and thus $\overline{\Delta\sigma}_E$) decreases while the dissipation remains unchanged. The lower bound for $\overline{\tau^{\text{ini}}}_E$ is given by either the condition $\eta_R > 0$ (positive radiation) or $\overline{\Delta\sigma}_E > 0$ (positive stress drop).

In constructing the scenarios of Figs 8(c) and (d), we keep the same experimentally motivated stress-slip curve and simply move the initial and final stress levels, for illustration purposes. This procedure results in quite complicated behaviours at the end of the ruptures. Figs 8(e) and (f) show streamlined versions of these scenarios, in which the average stress at the termination of substantial slip, $\overline{\tau}_{ter}$, and the final state of stress on the fault, $\overline{\tau^{\text{fin}}}_E$, are equal to each other. These simpler scenarios result in similar conclusions as those of Figs 8(c) and (d), since they have the same energy-based stress drops, and the modified parts of the energy balance are rather small. These streamlined versions make it clear that the case of Fig. 8(e) (as well as 8c) represents overshoot and the case of Fig. 8(f) (and 8d) represents a moderate undershoot, both of which are consistent with the observations on the radiation ratio.

An example of the averaged behaviour of shear stress with slip obtained in a dynamic rupture simulation is shown in Fig. 10. The dynamic rupture is simulated as a part of an earthquake sequence on a fault governed by a rate- and state-dependent friction, with additional dynamic weakening in the form of pore pressurization (Noda & Lapusta 2010b). This is the 7th event from fig. 8(b) of Noda & Lapusta (2010b). Note that the averaging of stress versus slip behaviour is done using the rigorous procedure described in Noda & Lapusta (2012), with the resulting average stress-slip curve reflecting the local stress versus slip behaviour on the fault while being scaled to preserve the dissipated energy and allowing for usual computations of strain energy change. The radiation ratio η_R for this event is 0.52. Note that one does not need to compute areas in this case to verify $\eta_R < 1$, as the entire dissipative stress curve is above the final stress, and $\eta_R < 1$ directly follows from Eg. (32).
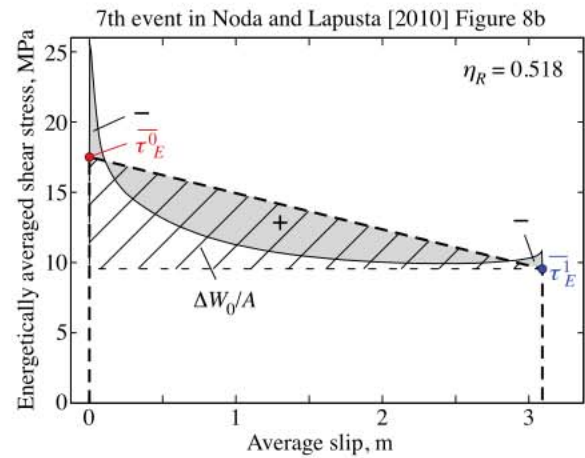

Figure 10. An example of the diagram showing energy partitioning obtained in a dynamic rupture simulation. The event is the 7th event in a sequence of earthquakes reported in fig. 8(b) of Noda & Lapusta (2010b). The radiation ratio of this event is 0.52.

4.2 Estimating moment-based and energy-based average stress drops from observations

To find the average stress drop from results of finite fault inversions, the effective rupture area A is estimated and then eq. (A8) or eq. (6) is used (e.g. Somerville *et al.* 1999; Venkataraman & Kanamori 2004). Hence, the estimated stress drop $\overline{\Delta\sigma}_M$ depends on the estimate of A. In particular, if the regions of small slip are excluded from the estimate of A, the obtained value for the stress drop increases from $\overline{\Delta\sigma}_M$. Since the energy-based stress drop $\overline{\Delta\sigma}_E$ is always larger than $\overline{\Delta\sigma}_M$, the question arises as to whether the rupture area can be defined so that the resulting moment-based stress drop approximates the larger energy-based one.

There is an uncertainty in the determination of the ruptured domain Σ and its area A. In practice, the ruptured domain obtained from an inversion often contains regions of near-zero slip. Such regions may not represent the actual source but rather be the result of the smoothness constraints often used in inversions (e.g. Harris & Segall 1987). As pointed out by Venkataraman & Kanamori (2004), different procedures can be used for determining the rupture area. Somerville *et al.* (1999) suggested a trimming criterion to shrink the ruptured domain from the support of a finite source inversion. Mai & Beroza (2000) used the autocorrelation length. In the absence of the finite source inversion, the length scale of the rupture area $A^{1/2}$ is estimated from the corner frequency, with assumptions on the rupture speed and the shape of the ruptured domain (e.g. Aki 1967; Brune 1970; Madariaga 1976).

Let us investigate how the moment-based and area-averaged stress drops vary for different definitions of the ruptured domain Σ_{th} based on a slip threshold, as in eq. (6). Fig. 11 shows such stress drops, which we denote by $\overline{\Delta\sigma}_{Mth}$ and $\overline{\Delta\sigma}_{Ath}$, as functions of the threshold th for a randomized model with $\nu = 1$ and $\chi = 0.3$ based on the circular crack with uniform stress drop. $\overline{\Delta\sigma}_{Mth}$ is estimated using eq. (6) even if Σ_{th} is not a connected region. If instead one modifies eq. (6) by starting with eq. (A8) and using E_1^{12} calculated for the exact shape of Σ_{th}, then the value of stress drop would be different. Although it is possible to solve such a mixed boundary problem in static elasticity, this may not be practical for observations since this would require recomputing the formula for each inversion. As th increases, Σ_{th} shrinks and A_{th} decreases, so that $\overline{\Delta\sigma}_{Mth}$ and $\overline{\Delta\sigma}_{Ath}$ increase. At the same time, $\overline{\Delta\sigma}_E$ is independent of the definition of the ruptured domain.
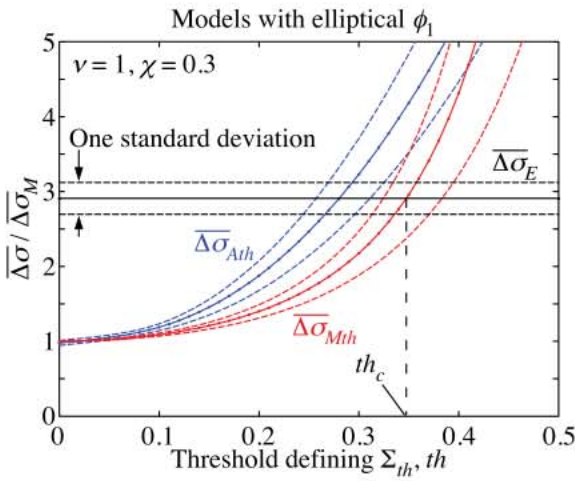
Figure 11. The dependence of $\overline{\Delta\sigma}_{Mth}$ and $\overline{\Delta\sigma}_{Ath}$ on the threshold th in defining Σ_{th} for randomized cases with $\nu = 1$ and $\chi = 0.3$ based on the circular crack model with uniform stress drop. At a certain value of th, $\overline{\Delta\sigma}_{Mth}$ becomes equal to $\overline{\Delta\sigma}_E$.
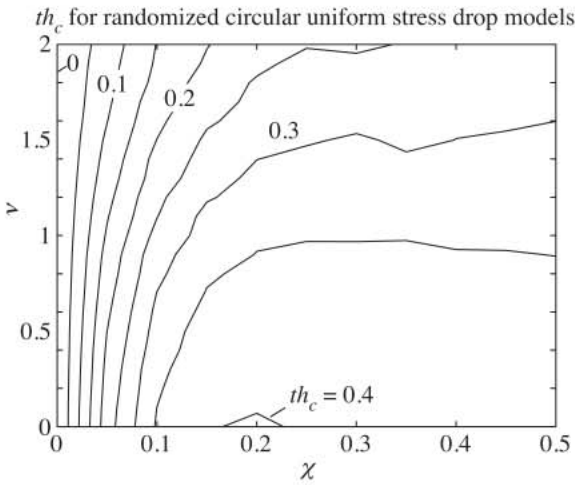

Figure 12. A contour plot of th_c as a function of ν and χ for randomized cases based on the circular crack models with uniform stress drops. The value of th_c is calculated every 0.1 in ν and 0.05 in χ. The axes are the same as in Fig. 6.

We observe that, at a certain value of th, $\overline{\Delta\sigma}_{Mth}$ becomes equal to $\overline{\Delta\sigma}_E$. Let us denote this value of th by th_c. If the ruptured domain is truncated using $th = th_c$, then $\overline{\Delta\sigma}_{Mth}$ would approximate $\overline{\Delta\sigma}_E$, and then ΔW_0 and hence the radiation ratio eq. (27) would be estimated correctly. For the case shown in Fig. 11 ($\nu = 1$ and $\chi = 0.3$), th_c has the mean value of 0.35, with the variance of 0.03, based on 100 random cases.

Fig. 12 shows the dependence of th_c on the parameters of slip heterogeneity ν and χ. For each parameter combination, the value of th_c is determined based on averaging 100 random cases. We find that $0.2 < th_c < 0.4$ for a broad range of the heterogeneity parameters, both in circular and rectangular cases. Hence, using th_c from that range for estimating the rupture area would be a reasonable choice for estimating stress drop values closer to the moment-based ones.

Note that the value of th_c depends on other characteristics of the slip distribution such as ϕ, the shape of Δu_1 before randomization. Fig. 13 shows the dependence of average stress drop measures on the threshold th for different ϕ. If ϕ reflects a characteristic feature of dynamic ruptures such as pulse-like propagation, the understanding
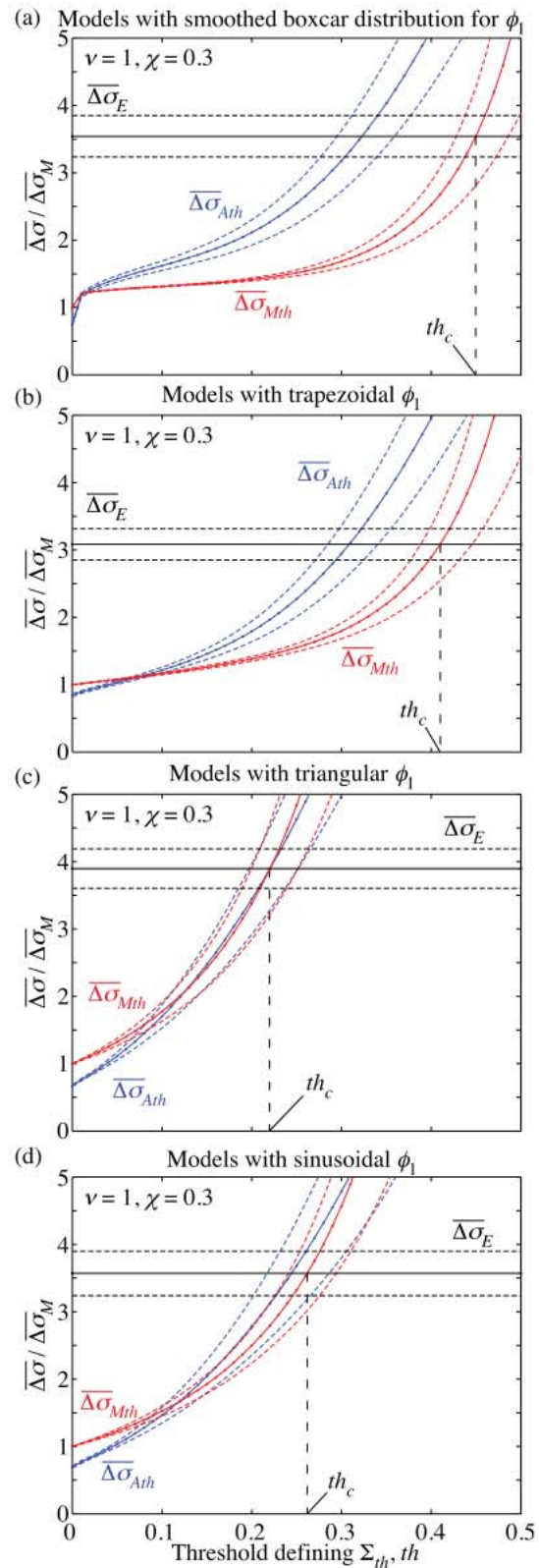
Figure 13. The dependence of $\overline{\Delta\sigma}_{Mth}$ and $\overline{\Delta\sigma}_{Ath}$ on the threshold th in defining Σ_{th} for randomized cases based on different original slip distributions: (a) smoothed boxcar, (b) trapezoidal, (c) triangular and (d) sinusoidal with $\nu = 1$ and $\chi = 0.3$.

of rupture dynamics would contribute to the estimation of th_c and hence to the estimation of the energy-based stress drop.

5 CONCLUSIONS

We have investigated three different approaches to averaging heterogeneous stress drop distributions following slip on a part of a planar interface and compared the resulting average stress drop measures: the moment-based $\overline{\Delta\sigma}_M$, the area-based $\overline{\Delta\sigma}_A$ and the energy-based $\overline{\Delta\sigma}_E$. Theoretically, the three measures are given by averages of a stress drop distribution over the planar interface with following different weighting functions: slip distribution of the corresponding uniform stress drop case for $\overline{\Delta\sigma}_M$, the boxcar function (which restricts the averaging to the ruptured domain only) for $\overline{\Delta\sigma}_A$ and the final slip distribution (which is potentially heterogeneous itself) for $\overline{\Delta\sigma}_E$. Practically, $\overline{\Delta\sigma}_M$ has been estimated from seismological observations in numerous studies, $\overline{\Delta\sigma}_A$ gives the difference in the average stress levels before and after rupture, and $\overline{\Delta\sigma}_E$ enters the calculations of partial strain energy change and radiation ratio (and hence considerations of energy partitioning).

To the best of our knowledge, this is the first study that explicitly introduces the energy-based average measure of stress drop, $\overline{\Delta\sigma}_E$, although its notion has been indirectly implied by the developments in Kostrov & Das (1988); Noda & Lapusta (2012). Unlike $\overline{\Delta\sigma}_M$ and $\overline{\Delta\sigma}_A$, $\overline{\Delta\sigma}_E$ does not depend on the definition of the ruptured domain Σ. Note that defining the ruptured domain in practice implies a criterion of what constitutes 'significant' slip, which is typically defined as a percentage of the maximum slip.

If the stress drop distribution is spatially uniform within the ruptured domain, the three average measures of stress drop are equal to each other. To compare the measures for non-uniform stress drop distributions, we consider both scenarios that are based on the uniform stress drop with a randomized addition, and scenarios that have different characteristic slip shape (non-elliptical). All scenarios have the same potency/moment, and hence the same $\overline{\Delta\sigma}_M$. We find that the three measures of the average stress drop are similar to each other for small levels of heterogeneity. Furthermore, the difference between the moment-based $\overline{\Delta\sigma}_M$ and area-based $\overline{\Delta\sigma}_A$ remains within a factor of two for all cases we have investigated.

However, we find substantial differences between $\overline{\Delta\sigma}_M$ and $\overline{\Delta\sigma}_E$, by a factor of up to 8 for the cases considered. This means that using the seismologically inferred stress drops for energy considerations can lead to substantial errors, since the uncertainty in the seismological estimates of stress drops is now combined with another significant factor (up to 8 in this study), resulting in the combined uncertainty factor for the partial strain energy change of one order of magnitude or more.

Fortunately, we find that $\overline{\Delta\sigma}_E \geq \overline{\Delta\sigma}_M$ always, the finding that we have proved theoretically. This means that using $\overline{\Delta\sigma}_M$ in the estimation of the partial strain energy change ΔW_0 and radiation ratio η_R results in systematic underestimation of ΔW_0 and hence systematic overestimation of η_R. This result suggests that the radiation ratios obtained by previous studies (Venkataraman & Kanamori (2004)) for a number of earthquakes may be overestimated. For some earthquakes, Venkataraman & Kanamori (2004) used a trimmed rupture area for estimating the stress drop. In those cases, the stress drop estimate is closer to $\overline{\Delta\sigma}_E$. However, their conclusion that most large earthquakes have the radiation ratio significantly smaller than one is further strengthened by our study, since the properly estimated values would be even smaller. Note that since the difference between $\overline{\Delta\sigma}_E$ and $\overline{\Delta\sigma}_M$ increases for more heterogeneous slip distributions,

the radiation ratios would decrease for cases with small-scale slip heterogeneity (assuming the same potency). We would like to emphasize that values $\eta_R > 1$ are theoretically allowed, but should be quite rare based on the observations.

The observation that the radiation ratio is typically smaller than one can be used to constrain the range of potential scenarios of dissipative stress evolution with slip, averaged over the entire fault. All scenarios in which the average dissipative shear stress rate is negative with slip satisfy $\eta_R < 1$, as do scenarios in which the average dissipative stress stays at or above the final average stress (resulting in overshoot or no undershoot). Some scenarios with substantial restrengthening (undershoot) may violate this observation. In particular, the scenario with high initial and final stress levels in comparison with the dynamic frictional resistance has η_R much larger than unity. However, undershoot scenarios in which the final stress is sufficiently low still satisfy $\eta_R < 1$.

The seismological moment-based estimate of stress drop depends on the definition of the ruptured domain Σ, which is uncertain in finite fault inversions due to areas of near-zero slip. Such areas may be present in inversions due to smoothing. If we define the ruptured domain by a threshold th with respect to the maximum slip, then the moment-based stress drop $\overline{\Delta\sigma}_{Mth}$ increases with the value of th. Selecting $th \sim 0.3$ results in a reasonable approximation to the energy-based stress drop $\overline{\Delta\sigma}_E$ for a wide range of randomized cases based on uniform stress drop models that we have studied.

One interesting finding is that even the characteristic overall shape of the slip distribution (without any smaller scale randomization) already notably affects the differences between the three average stress drop measures, especially between moment-based $\overline{\Delta\sigma}_M$ and energy-based $\overline{\Delta\sigma}_E$. Features of dynamic rupture nucleation, propagation, and arrest (unilateral versus bilateral, crack-like versus pulse-like, abruptness of rupture arrest, etc) can be interpreted as factors determining the characteristic slip distribution (elliptic versus triangular versus trapezoidal, etc). Hence differences in earthquake physics can contribute to systematic differences between the three average stress drop measures.

Our results suggest that improving our understanding of slip distribution during earthquakes, including its heterogeneity, is quite important for better constraints on energy partitioning.

ACKNOWLEDGEMENTS

REFERENCES

Abercrombie, R.E., 1995. Earthquake source scaling relationships from -1 to 5M_L using seismograms recorded at 2.5-km depth, *J. geophys. Res.*, **100**(B12), 24 015–24 036.

Aki, K., 1967. Scaling law of seismic spectrum, *J. geophys. Res.*, **72**, 1217–1231.

Allmann, B.P. & Shearer, P.M., 2009. Global variations of stress drop for moderate to large earthquakes, *J. geophys. Res.*, **114**, B01310, doi:10.1029/2008JB005821.

Andrews, D.J., 1980. A stochastic fault model, 1. Static case, *J. geophys. Res.*, **85**, 3867–3877.

Böse, M. & Heaton, T.H., 2010. Probablistic prediction of rupture length, slip and seismic ground motions for an ongoing rupture: implications for early warning for large earthquakes, *Geophys. J. Int.*, doi:10.1111/j.1365-246X.2010.04774.x.

Bouchon, M., 1997. The state of stress on some faults of the San Andreas systems as inferred from near-field strong motion data, *J. geophys. Res.*, **102**, 11 731–11 744.

Brune, J.N., 1970. Tectonic stress and the spectra of seismic shear waves from earthquakes, *J. geophys. Res.*, **75**, 4997–5009.

Cocco, M. & Tinti, E., 2008. Scale dependence in the dynamics of earthquake propagation: evidence from seismological and geological observations, *Earth plant. Sci. Lett.*, **273**, 123–131.

Cocco, M., Spudich, P. & Tinti, E., 2006. On the mechanical work absorbed on faults during earthquake ruptures, in *Earthquakes: Radiated Energy and the Physics of Faulting*, Vol. 170 of Geophys. Monogr. Ser., pp. 237–254, eds Abercrombie, R., McGarr, A., Kanamori, H. & Toro, G.D., AGU, Washington DC.

Dieterich, J.H., 1979. Modeling of rock friction. 1. Experimental results and constitutive equations, *J. geophys. Res.*, **84**(B5), 2161–2168.

Dieterich, J.H., 2007. Applications of rate- and state-dependent friction to models of fault slip and earthquake occurrence, in *Treatise on Geophysics*, Vol. 4, chap.4, pp. 107–129, ed. Kanamori, H., Elsevier, Amsterdam.

Eshelby, J.D., 1957. The determination of the elastic field of an ellipsoidal inclusion, and related problems, *Proc. Phys. Soc. A*, **241**, 376–391.

Fukuyama, E. & Mizoguchi, K., 2009. Constitutive parameters for earthquake rupture dynamics based on high-velocity friction tests with variable sliprate, *Int. J. Fract.*, doi:10.1007/s10704-009-9417-5.

Harris, R.A. & Segall, P., 1987. Detection of a locked zone at depht on the parkfield 1962, california segment of the san andreas fault, *J. geophys. Res.*, **92**, 7945–7962.

Hatzell, S., Liu, P. & Mendoza, C., 1996. The 1994 Northridge, California, earthquake: investigation of rupture velocity, risetime, and high-frequency radiation, *J. geophys. Res.*, **101**(B9), 20 091–20 108.

He, C., Wong, T.-F. & Beeler, N.M., 2003. Scaling of stress drop with recurrence interval and loading velocity for laboratory-derived fault strength relations, *J. geophys. Res.*, **108**, B1, doi:10.1029/2002JB001890.

Heaton, T.H., 1990. Evidence for and implications of self-healing pulses of slip in earthquake rupture, *Phys. Earth planet. Inter.*, **64**, 1–20.

Kanamori, H. & Anderson, D.L., 1975. Theoretical basis of some empirical relations in seismology, *Bull. seism. Soc. Am.*, **65**(5), 1073–1095.

Kanamori, H. & Rivera, L., 2006. Energy partitioning during an earthquake, in *Earthquakes: Radiated Energy and the Physics of Faulting*, Vol. 170 of Geophys. Monogr. Ser., pp. 3–13, eds Abercrombie, R., McGarr, A., Kanamori, H. & Toro, G.D., AGU, Washington DC.

Knopoff, L., 1958. Energy release in earthquakes, *Geophys. J.*, **1**, 44–52.

Kostrov, B.V. & Das, S., 1988. *Principles of Earthquake Source Mechanics*, Cambridge University Press, Cambridge.

Lapusta, N. & Liu, Y., 2009. 3d boundary-integral modeling of spontaneous earthquake sequences and aseismic slip, *J. geophys. Res.*, **114**, B09303, doi:10.1029/2008JB005934.

Lavallée, D., Liu, P. & Archuleta, R.J., 2006. Stochastic model of heterogeneity in earthquake slip spatial distributions, *Geophys. J. Int.*, **165**, 622–640.

Liu, P. & Archuleta, R.J., 2000. Inversions for kinematic source parameters of 1994 Northridge earthquake using a three dimensional velocity structure, *Seismol. Res. Lett.*, **71**, 237.

Liu-Zeng, J., Heaton, T. & DiCaprio, C., 2005. The effect of slip variability on earthquake slip-length scaling, *Geophys. J. Int.*, **162**, 841–849.

Madariaga, R., 1976. Dynamics of an expanding circular fault, *Bull. seism. Soc. Am.*, **66**, 639–667.

Madariaga, R., 1979. On the relation between seismic moment and stress drop in the presence of stress and strength heterogeneity, *J. geophys. Res.*, **84**, 2243–2250.

Mai, M. & Beroza, G.C., 2000. Source scaling properties from finite-fault-rupture models, *Bull. seism. Soc. Am.*, **90**, 604–615.

Manighetti, I., Campillo, M., Sammis, C., Mai, P.M. & King, G., 2005.

Evidence for self-similar, triangular slip distributions on earthquakes: implications for earthquake and fault mechanics, *J. geophys. Res.*, **110**, B05302, doi:10.1029/2004JB003174.

Marone, C., 1998. The effect of loading rate on static friction and the rate of faulr healing during the earthquake cycle, *Nature*, **391**, 69–72.

McGarr, A., 1999. On relating apparent stress to the stress causing earthquake fault slip, *J. geophys. Res.*, **104**(B2), 3003–3011.

Minson, S.E., 2010. A Bayesian approach to earthquake source studies, *PhD thesis*, California Institute of Technology.

Noda, H. & Lapusta, N., 2010a. 3D simulations of long-term fault slip with dynamic weakening: relation between locked patches and earthquake-induced stress changes, Workshop on Earthquake Source Dynamics: Data and Data-constrained Numerical Modeling, Smolenice Castle, Slovakia, 2010 June 27 to July 1.

Noda, H. & Lapusta, N., 2010b. Three-dimensional earthquake sequence simulations with evolving temperature and pore pressure due to shear heating: effect of heterogeneous hydraulic diffusivity, *J. geophys. Res.*, **115**, B12314, doi:10.1029/2010JB007780.

Noda, H. & Lapusta, N., 2012. On averaging interface response during dynamic rupture and energy partitioning diagrams for earthquakes, *J. Appl. Mech.*, **79**, doi:10.1115/1.4005964.

Noda, H., Dunham, E.M. & Rice, J.R., 2009. Earthquake ruptures with thermal weakening, and the operation of major faults at low overall stress levels, *J. geophys. Res.*, **114**, B07302, doi:10.1029/2008JB006143.

Parsons, I.D., Hall, J.F. & Lyzenga, G.A., 1988. Relationships between the averaged offset and the stress drop for two- and three-dimentional faults, *Bull. seism. Soc. Am.*, **78**(2), 931–945.

Pavic, R., Koller, M.G., Bard, P.Y. & Lacave-Lachet, C., 2000. Ground motion prediction with the empirical green's function technique: an assesment of uncertainties and confidence level, *J. Seism.*, **4**, 59–77.

Perrin, G., Rice, J.R. & Zheng, G., 1995. Self-healing slip pulse on a frictional interface, *J. Mech. Phys. Solids*, **43**, 1461–1495.

Rice, J.R., 1993. Spatio-temporal complexity of slip on a fault, *J. geophys. Res.*, **98**, 9885–9907.

Rice, J.R., 2006. Heating and weakening of faults during earthquake slip, *J. Geophys. Res.*, **111**(B5), B05311, doi:10.1029/2005JB004006.

Somerville, P.G. *et al.*, 1999. Characteizing crustal earthquake slip models for the predisction of strong ground motion, *Seismol. Res. Lett.*, **70**, 59–80.

Sone, H. & Shimamoto, T., 2009. Frictional resistance of faults during accelerating and decelerating earthquake slip, *Nat. Geosci.*, **2**, 705–708.

Starr, A.T., 1928. Slip in a crystal and rupture in a solid due to shear, *Math. Proc. Cambridge Philos. Soc.*, **24**, 489–500.

Tullis, T.E., 2007. Friction of rock at earthquake slip rates, in *Treatise on Geophysics*, Vol. 4, chap. 5, pp. 131–152, ed. Kanamori, H., Elsevier, Amsterdam.

Venkataraman, A. & Kanamori, H., 2004. Observational constraints onthe fracture energy of subduction zone earthquakes, *J. geophys. Res.*, **109**, B05302, doi:10.1029/2003JB002549.

Ward, S.N., 2004. Earthquake simulation by restricted random walks, *Bull. seism. Soc. Am.*, **95**(36), 2079–2089.

Zheng, G. & Rice, J.R., 1998. Conditions under which velocity-weakening friction allows a self-healing versus a cracklike mode of rupture, *Bull. seism. Soc. Am.*, **88**, 1466–1483.

APPENDIX A: EXPRESSION OF MOMENT-BASED STRESS DROP BY MADARIAGA 1979

Madariaga (1979) discussed the relation between models of uniform and heterogeneous stress drop distributions and pointed out that the seismologically estimated stress drop is not, in general, equal to the area-averaged stress drop. The seismic moment tensor M_{ij} is written as

$$M_{ij} = \mu \int_{\Sigma} (\Delta u_i n_j + \Delta u_j n_i)\, dS, \qquad (A1)$$

where Δu_i and n_i are the *i*th components of Δu and the unit normal vector n to the fault, respectively. By using the elastic reciprocity theorem, Madariaga (1979) showed that M_{ij} can be written in terms of stress drop distribution $\Delta \sigma(x_1, x_3)$ as

$$M_{ij} = \int_\Sigma \Delta \sigma_k \left(E_k^{ij} + E_k^{ji} \right) dS, \tag{A2}$$

where E_k^{ij} is the *k*th component of the slip vector due to stress drop ΔT^{ij} on Σ such that its *l*th component is given by

$$\Delta T_l^{ij} = \mu n_j \delta_{li}. \tag{A3}$$

In our study, the fault has a uniform unit normal vector $n = e_2$ (i.e. $n_1 = n_3 = 0$ and $n_2 = 1$), and the overall slip direction is e_1. In this case, the only non-zero components of the seismic moment tensor are

$$M_0 = M_{12} = M_{21} = \mu \int_\Sigma \Delta u_1 \, dS. \tag{A4}$$

From eqs (A2) and (A3),

$$M_0 = \int_\Sigma \Delta \sigma_k E_k^{12} \, dS, \tag{A5}$$

where E_k^{12} ($k = 1, 3$) is the *k*th component of the slip distribution due to uniform stress drop by the shear modulus μ on Σ in the direction of e_1.

Slip functions E^{12} depend on the domain Σ. For a circular crack model with the radius r, one has (Eshelby 1957)

$$E_1^{12} = \frac{24}{7\pi} r \left(1 - r'^2/r^2 \right)^{1/2}, \quad E_2^{12} = E_3^{12} = 0, \tag{A6}$$

where r' is the radial coordinate measured from the centre of the crack. Note that the Poisson's ratio is assumed to be 1/4. There is no known analytical expression of E^{12} for rectangular crack models. Parsons *et al.* (1988) numerically calculated the slip functions for specific aspect ratios. In this study, we examine circular ruptured domains and rectangular ruptured domains with aspect ratios $\alpha = 1, 4$ and 16. In the rectangular cases, we calculate E^{12} numerically by conducting quasi-dynamic rupture propagation calculations for a traction-free rupture domain with uniform initial stresses (Appendix B1).

Note that from eq. (A5), if the stress drop is uniform and equal to $\overline{\Delta \sigma}_M e_1$, then

$$\overline{\Delta \sigma}_M = \frac{M_0}{\int_\Sigma E_1^{12} \, dS}. \tag{A7}$$

In practice, even when the stress change on the fault is not uniform, seismologists often estimate a stress drop using eq. (A7). We call $\overline{\Delta \sigma}_M$ moment-based or seismologically estimated stress drop. It follows from eqs (A5) and (A7) that $\overline{\Delta \sigma}_M$ is given by

$$\overline{\Delta \sigma}_M = \frac{\int_S \Delta \sigma \cdot w \, dS}{\int_S e_1 \cdot w \, dS}; \quad w = E^{12}. \tag{A8}$$

where w is the weighting function. The formulae eq. (4) are obtained by evaluating the spatial integrations in eq. (A7).

APPENDIX B: RECTANGULAR RUPTURES

B1 Slip distributions for uniform stress drop models

The slip distribution due to a uniform stress drop over a certain region is a solution to a mixed boundary-value problem. The analytic

solution for such a problem is not always known. The analytic solution for a 2-D planar crack was derived by Starr (1928), and the solutions for the circular and elliptical cracks were derived by Eshelby (1957). Parsons *et al.* (1988) calculated solutions for rectangular cracks with different aspect ratios and burial depth using a finite element method and then derived formulae similar to eq. (6). Those results have been widely used in estimation of stress drops in seismology.

In this work, slip distributions ϕ_1 and ϕ_3 for rectangular ruptures with uniform stress drop have been computed by conducting quasi-dynamic simulations using the spectral boundary integral method (Rice 1993). Adaptive time stepper is used which minimizes the L_2 norm of the slip rate (or, equivalently, traction in the quasi-static problem) inside the ruptured domain Σ. Let us select the reference state of linear elasticity such that no slip corresponds to zero shear stress on the fault S, and assume uniform stress drop μ inside Σ. At the *n*th step, we have a slip distribution $(\phi_{1(n)}, \phi_{2(n)})$ inside Σ. The static stress field $(f_{1(n)}, f_{2(n)})$ due to that slip distribution is calculated using eq. (25) as

$$\begin{bmatrix} F[f_{1(n)}] \\ F[f_{2(n)}] \end{bmatrix} = -\frac{\mu}{2k} \begin{bmatrix} k_1^2/(1-\nu_p) + k_3^2 & k_1 k_3 \nu_p/(1-\nu_p) \\ k_1 k_3 \nu_p/(1-\nu_p) & k_1^2 + k_3^2/(1-\nu_p) \end{bmatrix}$$
$$\times \begin{bmatrix} F[\phi_{1(n)}] \\ F[\phi_{2(n)}] \end{bmatrix}, \tag{B1}$$

where $F[\ ]$ is the Fourier coefficient that corresponds to a wavenumber vector (k_1, k_3), k is the absolute value of that vector, and ν_p is Poisson's ratio which is assumed to be 1/4. Note that similarly to the main part of this paper, we assume spatial periodicity with the period which is four times larger than the rupture length. From the quasi-dynamic approximation (Rice 1993), the corresponding slip rate $(V_{1(n)}, V_{2(n)})$ is

$$\begin{bmatrix} V_{1(n)} \\ V_{2(n)} \end{bmatrix} = \frac{1}{\eta} \left(\begin{bmatrix} f_{1(n)} \\ f_{2(n)} \end{bmatrix} - \begin{bmatrix} -\Delta \sigma_1 \\ 0 \end{bmatrix} \right), \tag{B2}$$

where $\eta = \mu/(2c_s)$. The stress drop distribution is:

$$\Delta \sigma_1 = \begin{cases} \mu & \text{inside } \Sigma \\ 0 & \text{outside } \Sigma \end{cases} \tag{B3}$$

The rate of change of the static stress field is

$$\begin{bmatrix} F[\dot{f}_{1(n)}] \\ F[\dot{f}_{2(n)}] \end{bmatrix} = -\frac{\mu}{2k} \begin{bmatrix} k_1^2/(1-\nu_p) + k_3^2 & k_1 k_3 \nu_p/(1-\nu_p) \\ k_1 k_3 \nu_p/(1-\nu_p) & k_1^2 + k_3^2/(1-\nu_p) \end{bmatrix}$$
$$\times \begin{bmatrix} F[V_{1(n)}] \\ F[V_{2(n)}] \end{bmatrix}. \tag{B4}$$

In an explicit time integration with a time step Δt_n, the distributions of slip and static stress are updated as

$$\begin{bmatrix} \phi_{1(n+1)} \\ \phi_{2(n+1)} \end{bmatrix} = \begin{bmatrix} \phi_{1(n)} \\ \phi_{2(n)} \end{bmatrix} + \Delta t_n \begin{bmatrix} V_{1(n)} \\ V_{2(n)} \end{bmatrix}, \tag{B5}$$

$$\begin{bmatrix} f_{1(n+1)} \\ f_{2(n+1)} \end{bmatrix} = \begin{bmatrix} f_{1(n)} \\ f_{2(n)} \end{bmatrix} + \Delta t_n \begin{bmatrix} \dot{f}_{1(n)} \\ \dot{f}_{2(n)} \end{bmatrix}. \tag{B6}$$

In order to minimize the norm of the mismatch in the static stress field at the $(n + 1)$th step:

$$L_2 = \sum_{(x_1, x_3) \in \Sigma} \left\{ (f_{1(n+1)} + \mu)^2 + f_{2(n+1)}^2 \right\}, \tag{B7}$$
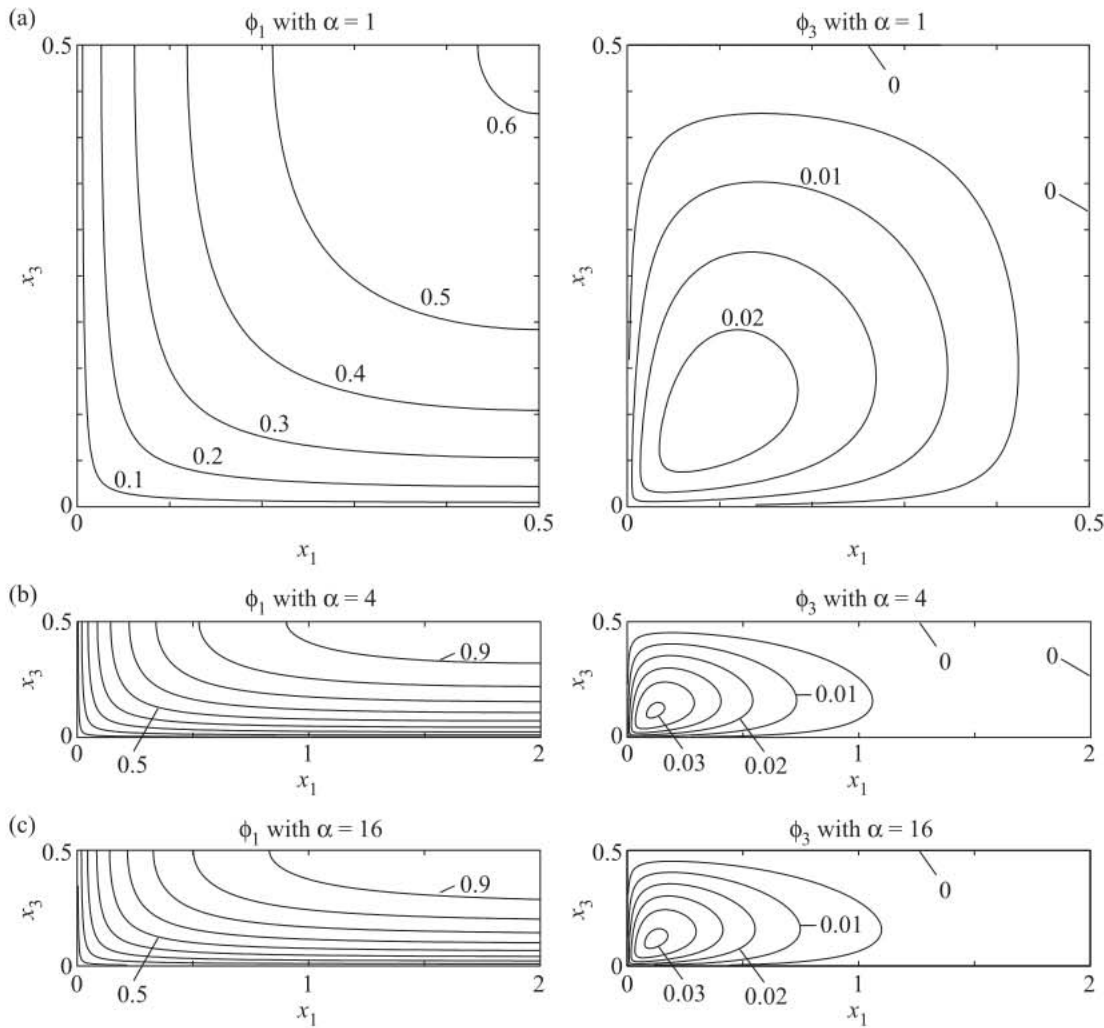
Figure B1. Slip distribution due to a uniform stress drop by μ in the direction of x_1 for rectangular domains with different aspect ratios: (a) $\alpha = 1$, (b) $\alpha = 4$, (c) $\alpha = 16$. The left-hand side and right-hand side columns show distribution of ϕ_1 and ϕ_3, respectively. The domains have unit widths (dimension of the fault in the x_3 direction). Because of symmetries of ϕ_1 and ϕ_3, only a quarter of the domain is shown for $\alpha = 1$ and $\alpha = 4$. For $\alpha = 16$, only the region near the end of the rupture is shown for convenience. Note that one of the corners of the fault is located at $(x_1, x_3) = (0, 0)$ in all cases. The centre of the fault is located at $(0.5, 0.5)$ in (a), $(2, 0.5)$ in (b) and $(8, 0.5)$ in (c).

the time step Δt_n is selected such that

$$\Delta t_n = -\frac{\sum_{(x_1, x_3) \in \Sigma} \{(f_{1(n)} + \mu) f'_{1(n)} + f_{2(n)} f'_{2(n)}\}}{\sum_{(x_1, x_3) \in \Sigma} \{f'^2_{1(n)} + f'^2_{2(n)}\}} \tag{B8}$$

The series of slip distributions $(\phi_{1(n)}, \phi_{2(n)})$ $(n = 1, 2, 3, \ldots)$ is not meant to be an approximation of any physical process but rather this is a way to converge to the static solution We iterate this step until the maximum value of $|f_{1(n)} + \mu|$ and $|f_{2(n)}|$ becomes smaller than $10^{-6}\mu$.

Fig. B1 shows the resulting slip distributions in the uniform stress drop models for rectangular ruptures with the aspect ratios $\alpha = 1$, 4, and 16. ϕ_3 is not uniformly zero, although its amplitude is much smaller than that of ϕ_1. Note that E^{12} is equal to (ϕ_1, ϕ_3). Spatial integration of E^{12}_1 yields $C = 2.53$, 3.02 and 5.21 in eq. (A8) for $\alpha = 1$, 4 and 16, respectively. Our calculation agrees with Parsons *et al.* (1988) who reported $C = 2.55$ for a square rupture (i.e. $\alpha = 1$) based on a finite-element calculation. Because we assume spatial periodicity (with the size of the repeated domain four times larger than the ruptured domain) and Parsons *et al.* (1988) assumed large

enough burial depth, our estimation of C is expected to be smaller because of the stress concentration due to periodic replications. The mismatch is negligibly small, and the comparison between different averaged stress drops is not affected by the existence of periodicity.

B2 Effect of randomization for rectangular ruptures

The rectangular uniform stress drop models described in the previous appendix are randomized using the same approach as for the circular ruptures, based on eq. (23). Figs B2, B3 and B4 show distributions of Δu_1 and $\Delta \sigma_1$ for the rectangular domains with aspect ratios $\alpha = 1$, 4 and 16, respectively.

Fig. B5 shows $\overline{\Delta \sigma}_E / \overline{\Delta \sigma}_M$ for rectangular cases. Similarly to the circular cases, introduction of heterogeneity increases $\overline{\Delta \sigma}_E / \overline{\Delta \sigma}_M$ from 1. As α increases, $\overline{\Delta \sigma}_E / \overline{\Delta \sigma}_M$ becomes less dependent on χ at large v. This can be explained by the following consideration. If a Fourier mode with much a longer wavelength than the width of the rupture is dominant along the rupture length (e.g. the cases with

$\nu = 2$ and $\alpha = 16$ shown in Fig. B4), then the distributions of slip and stress drop can be approximated by

$$\Delta u_1 \approx \frac{\overline{\Delta\sigma}_M}{\mu}\phi_1[1 + \epsilon \sin(k_1 x_1 + c)], \qquad (B9)$$

$$\Delta\sigma_1 \approx \overline{\Delta\sigma}_M[1 + \epsilon \sin(k_1 x_1 + c)], \qquad (B10)$$

where ϵ is the amplitude of the sinusoidal perturbation and c is a constant. In this approximation, $\overline{\Delta\sigma}_E$ becomes

$$\overline{\Delta\sigma}_E = \frac{\int_S \Delta\sigma_1 \Delta u_1 \, dS}{\int_S \Delta u_1 \, dS} \approx \overline{\Delta\sigma}_M. \qquad (B11)$$

Therefore, if ν is large enough so that only the long wavelength components parallel to domain lengths are significant, $\overline{\Delta\sigma}_E$ is expected to be near $\overline{\Delta\sigma}_M$.

The threshold values for truncating the ruptured domain so that the moment-based stress drop becomes a good approximation of the energy-based one are shown in Fig. B6. The results suggest that $th_c \sim 0.2 - 0.4$ unless the slip distribution is very heterogeneous, similarly to the circular models, although it should be noted that th_c depends on the characteristic slip distributions ϕ_1 and ϕ_3.
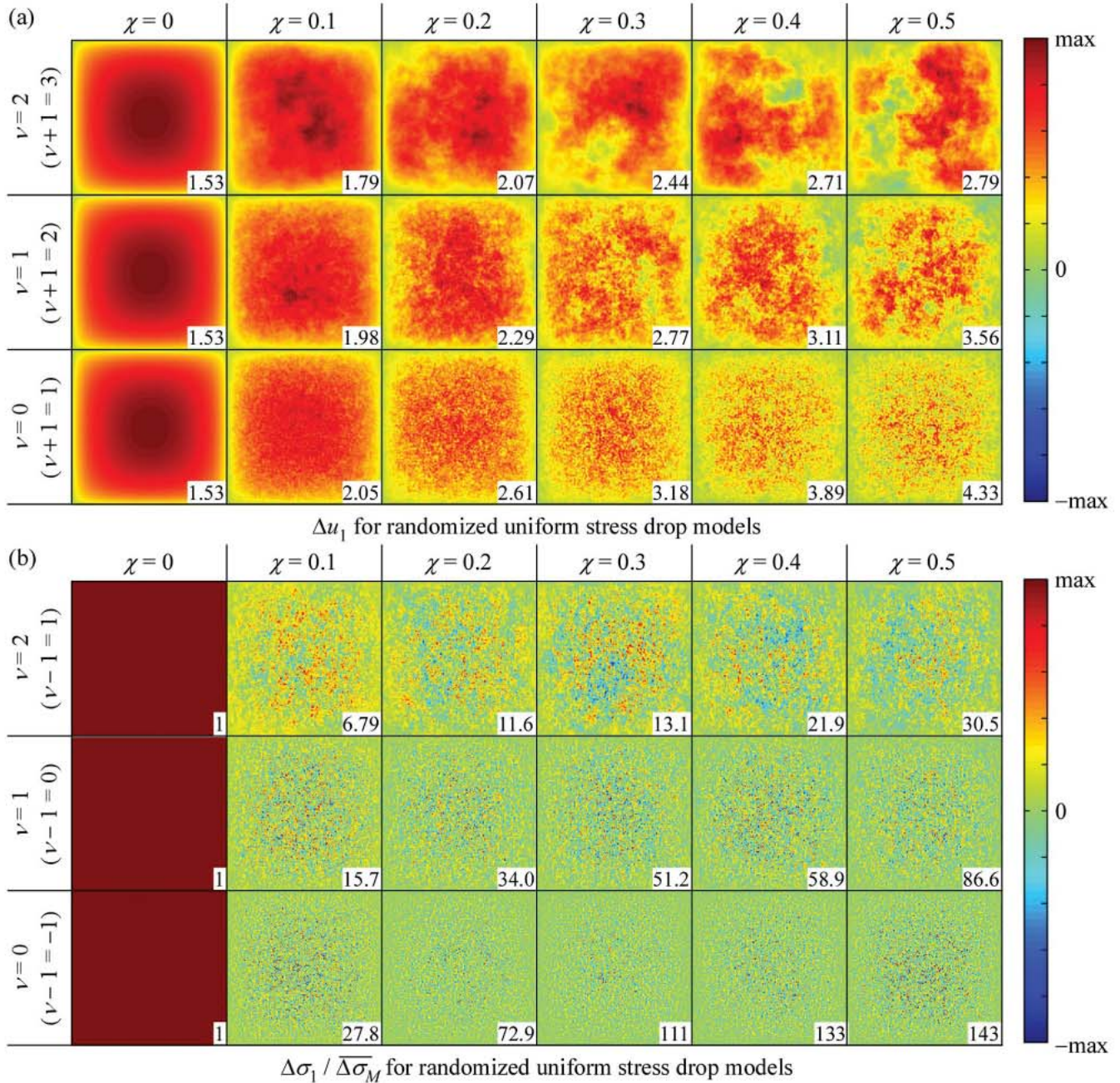

Figure B2. Examples of distributions of (a) Δu_1 and (b) $\Delta\sigma_1$ for randomized models based on square ruptured domains with uniform stress drop. The number at the bottom right of each panel indicates the maximum value of the quantity plotted. The sides of the square and the potency are normalized to one.
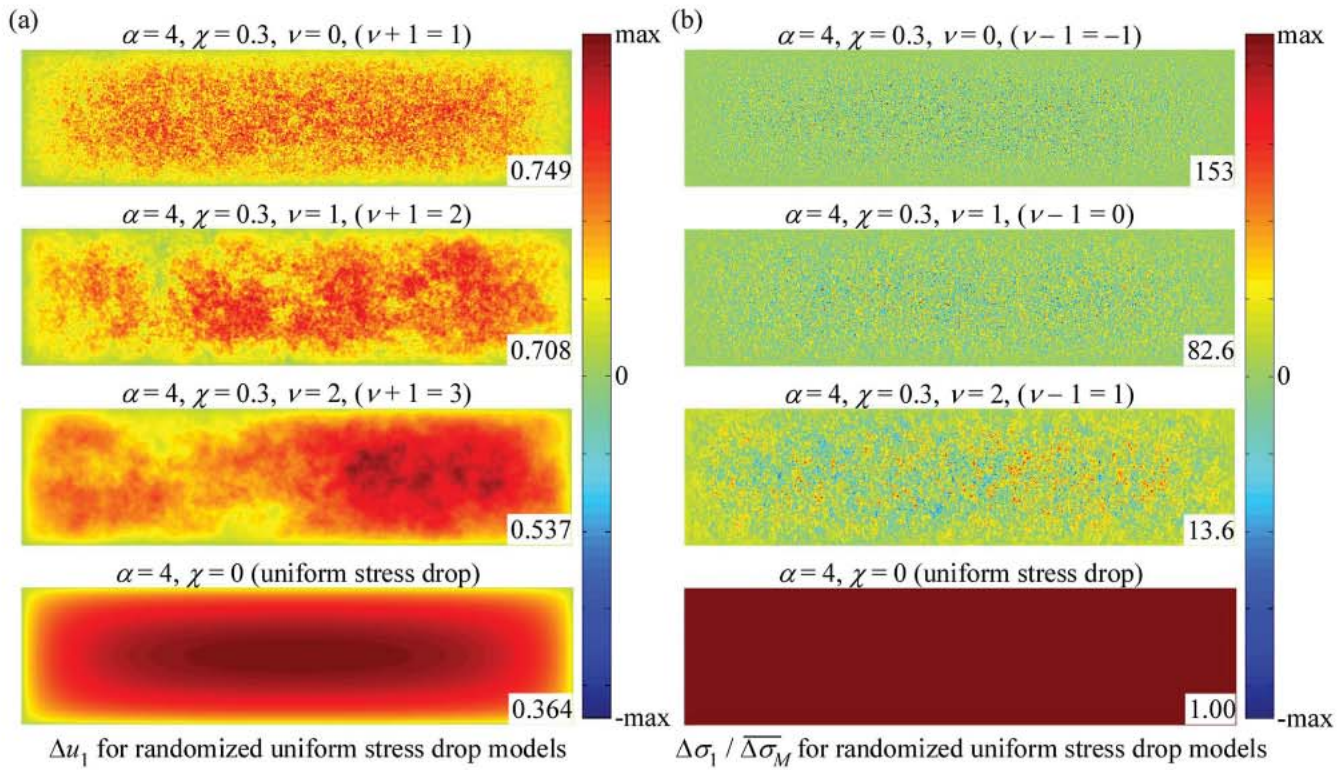
Figure B3. Examples of distributions of (a) Δu_1 and (b) $\Delta \sigma_1$ for randomized models based on rectangular ruptured domains (aspect ratio $\alpha = 4$) with uniform stress drop. The number at the bottom right of each panel indicates the maximum value of the quantity plotted. The shorter sides of the rectangular and the potency are normalized to one.
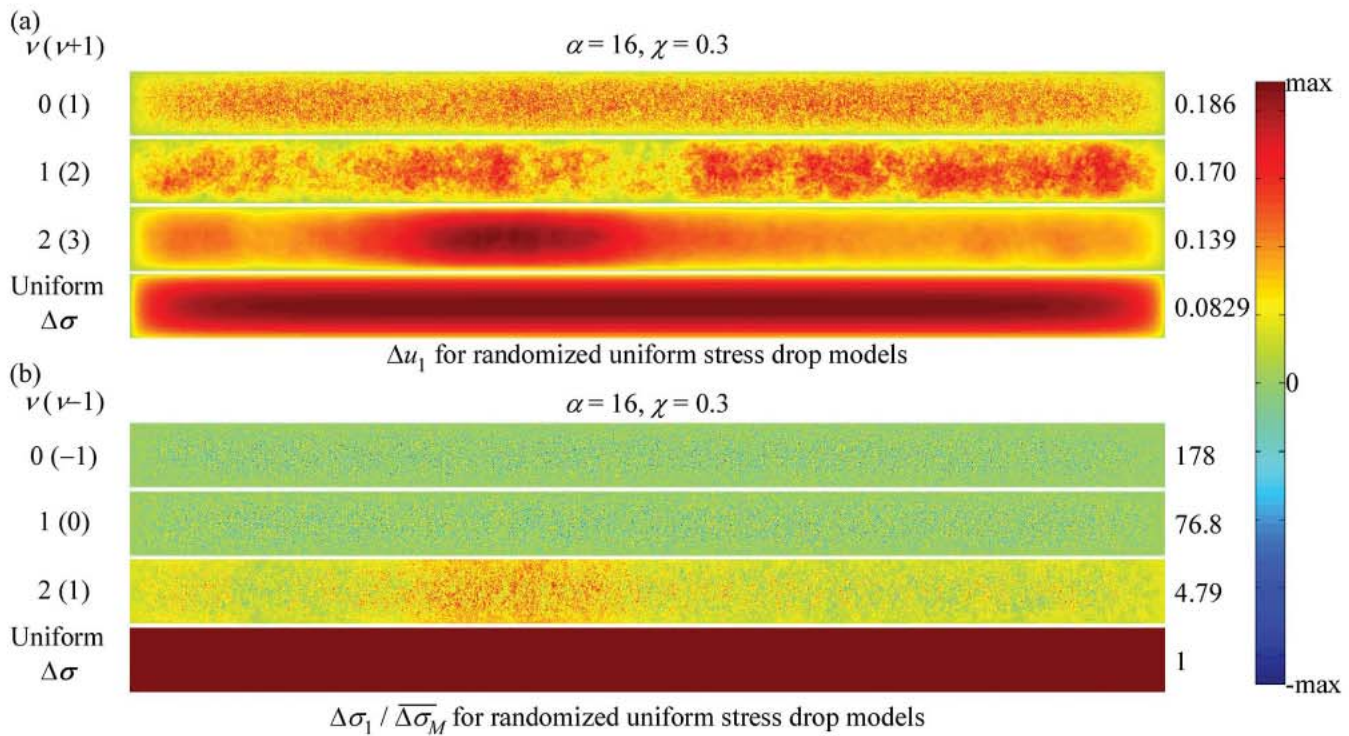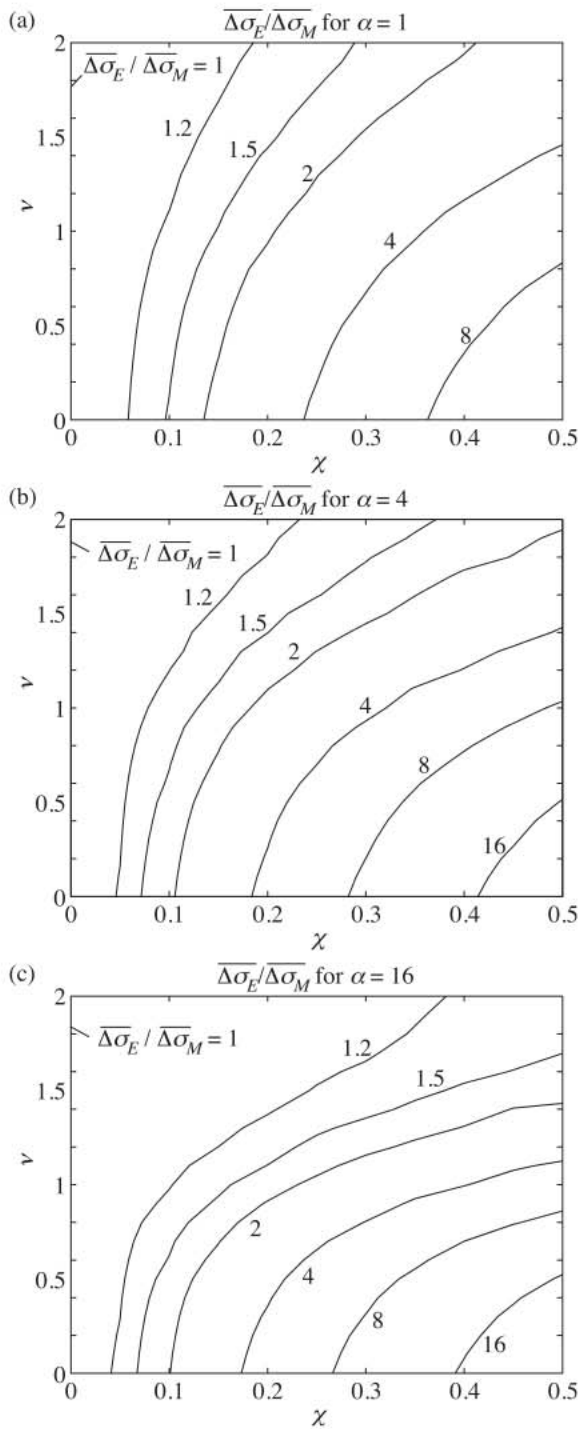

Figure B4. Examples of distributions of (a) Δu_1 and (b) $\Delta \sigma_1$ for randomized models based on rectangular ruptured domains (aspect ratio $\alpha = 16$) with uniform stress drop. The number at the bottom right of each panel indicates the maximum value of the quantity plotted. The shorter sides of the rectangular and the potency are normalized to one.

Figure B5. $\overline{\Delta\sigma}_E/\overline{\Delta\sigma}_M$ as a function of parameters characterizing roughness of the randomized models based on rectangular ruptures with uniform stress drop: (a) $\alpha = 1$, (b) $\alpha = 4$, (c) $\alpha = 16$.
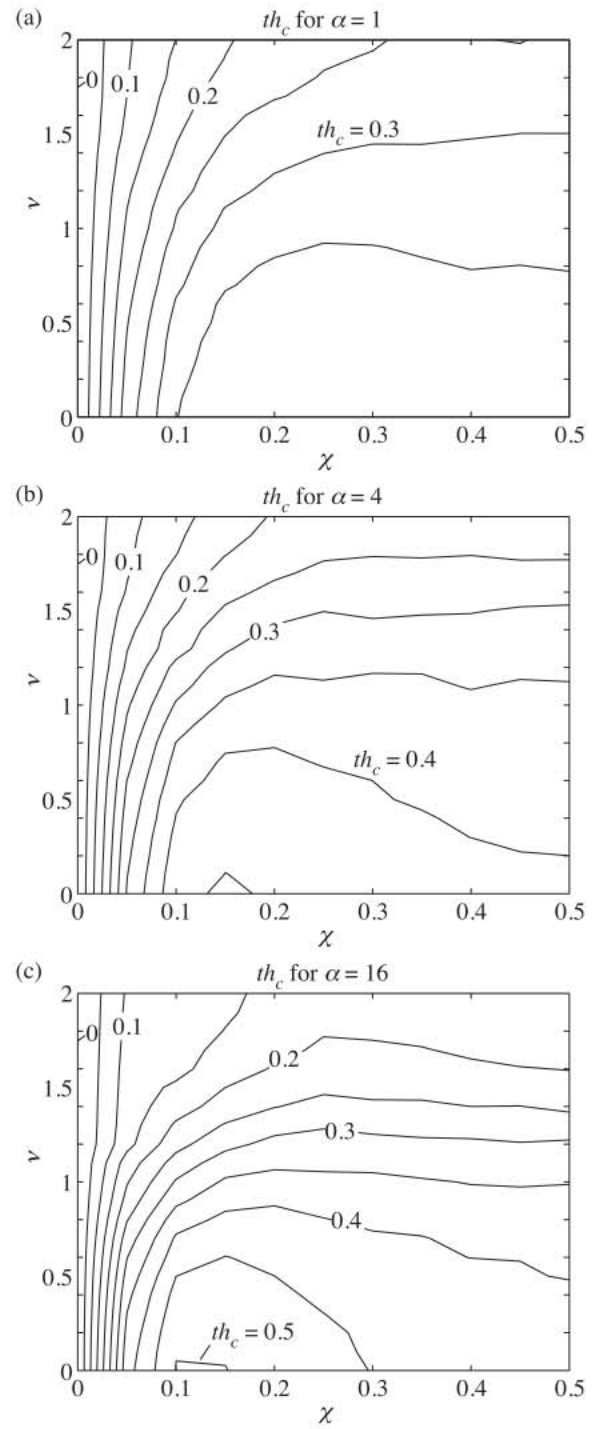
Figure B6. The threshold th_c which yield $\overline{\Delta\sigma}_E = \overline{\Delta\sigma}_{Mth}$ for randomized models based on rectangular ruptures with uniform stress drop: (a) $\alpha = 1$, (b) $\alpha = 4$, (c) $\alpha = 16$.

APPENDIX C: PROOF OF $\overline{\Delta\sigma}_E \geq \overline{\Delta\sigma}_M$

First, let us point out that partial strain energy change is a non-negative quantity. From eq. (17), the partial strain energy change ΔW_0 is a function of slip distribution $\Delta\boldsymbol{u}$,

$$\Delta W_0 = \frac{1}{2}\int_\Sigma \Delta\boldsymbol{\sigma}\cdot\Delta\boldsymbol{u}\,\mathrm{d}S, \tag{C1}$$

where $\Delta\boldsymbol{\sigma}$ is a linear function of $\Delta\boldsymbol{u}$ given by eq. (25). ΔW_0 is the volume integral of the strain energy density distribution due to $\Delta\boldsymbol{u}$ added to the stress-free configuration,

$$\Delta W_0 = \int_V W(\Delta\boldsymbol{\epsilon})\,dV, \tag{C2}$$

where $\Delta\epsilon$ is the strain distribution due to Δu on the fault and W is the strain energy function. Because W is positive definite, ΔW_0 is non-negative for any Δu,

$$\Delta W_0(\Delta u) \geq 0 \quad \text{for all} \quad \Delta u \tag{C3}$$

Any slip distribution can be expressed as a sum of a uniform stress drop model and the deviation from it which has zero potency. Let us consider a uniform stress drop model, with Δu_u and $\Delta\sigma_u$, and a perturbation to it, Δu_p and $\Delta\sigma_p$ such that the support of Δu_p is Σ and and the potency of the perturbation is zero,

$$\int_\Sigma \Delta u_p \, dS = 0. \tag{C4}$$

All the other conventions are the same as in the problem setup of Section 2. The partial strain energy changes due to Δu_u and Δu_p separately are given by

$$\Delta W_{0u} = \frac{1}{2} \int_\Sigma \Delta\sigma_u \cdot \Delta u_u \, dS \geq 0, \tag{C5}$$

and

$$\Delta W_{0p} = \frac{1}{2} \int_\Sigma \Delta\sigma_p \cdot \Delta u_p \, dS \geq 0. \tag{C6}$$

The partial strain energy change due to the sum of the uniform stress drop model and the perturbation is

$$\begin{aligned}
\Delta W_{0up} &= \frac{1}{2} \int_\Sigma (\Delta\sigma_u + \Delta\sigma_p) \cdot (\Delta u_u + \Delta u_p) \, dS \\
&= \Delta W_{0u} + \Delta W_{0p} + \frac{1}{2} \int_\Sigma \Delta\sigma_u \cdot \Delta u_p \, dS \\
&\quad + \frac{1}{2} \int_\Sigma \Delta\sigma_p \cdot \Delta u_u \, dS.
\end{aligned} \tag{C7}$$

Because $\Delta\sigma_u$ is uniform and the perturbation has zero potency (eq. C4), the third term in eq. (C7) is zero,

$$\frac{1}{2} \int_\Sigma \Delta\sigma_u \cdot \Delta u_p \, dS = \frac{1}{2}\Delta\sigma_u \cdot \int_\Sigma \Delta u_p \, dS = 0. \tag{C8}$$

Using the elastic reciprocity theorem, the fourth term is identical to the third term which is zero,

$$\frac{1}{2} \int_\Sigma \Delta\sigma_p \cdot \Delta u_u \, dS = \frac{1}{2} \int_\Sigma \Delta\sigma_u \cdot \Delta u_p \, dS = 0. \tag{C9}$$

Therefore, eq. (C7) leads to

$$\Delta W_{0up} = \Delta W_{0u} + \Delta W_{0p}. \tag{C10}$$

Because of the non-negativeness of ΔW_{0p} (eq. C3), we can conclude,

$$\Delta W_{0up} \geq \Delta W_{0u}. \tag{C11}$$

This means that if the support of the slip distribution and the potency (or the seismic moment) is preserved, then the uniform stress drop model minimizes the partial strain energy change ΔW_0.

Now let us use this result to compare $\overline{\Delta\sigma}_E$ and $\overline{\Delta\sigma}_M$ for the case with slip distribution $\Delta u_{up} = \Delta u_u + \Delta u_p$. From eq. (18), one has

$$\Delta W_{0up} = \frac{1}{2}\overline{\Delta\sigma}_E \overline{\Delta u_{up1}} A = \frac{1}{2}\overline{\Delta\sigma}_E \overline{\Delta u_{u1}} A. \tag{C12}$$

The second equality in eq. (C12) holds because the cases with Δu_{up} and Δu_u have the same potency/moment (by construction); this also means that they have the same moment-based stress drop $\overline{\Delta\sigma}_M$. Furthermore, for the uniform stress drop case with Δu_u, all three average measures of stress drop considered in this study are equal, and hence the moment-based stress drop can be used to find ΔW_{0u},

$$\Delta W_{0u} = \frac{1}{2}\overline{\Delta\sigma}_M \overline{\Delta u_{u1}} A. \tag{C13}$$

Eqs (C11), (C12) and (C13) immediately yield

$$\overline{\Delta\sigma}_E \geq \overline{\Delta\sigma}_M. \tag{C14}$$